HELSINKI INSTITUTE OF PHYSICS INTERNAL REPORT SERIES

HIP-2014-04

# Implications of Dark Matter in Supersymmetric Models

Lasse Leinonen

Helsinki Institute of Physics
University of Helsinki
Finland

ACADEMIC DISSERTATION

*To be presented, with the permission of the Faculty of Science of the University of Helsinki, for public criticism in the Auditorium (CK112) at Exactum, Gustaf Hällströmin katu 2B, Helsinki, on the 28th of January 2015 at 12 o'clock.*

Helsinki 2015

ISBN 978-952-10-8120-0 (print)
ISBN 978-952-10-8121-7 (pdf)
ISSN 1455-0563
http://ethesis.helsinki.fi
Unigrafia
Helsinki 2015

Lasse Leinonen: Implications of Dark Matter in Supersymmetric Models,
University of Helsinki, 2015, 77 pages,
Helsinki Institute of Physics, Internal Report Series, HIP-2014-04,
ISBN 978-952-10-8120-0,
ISSN 1455-0563.

# Abstract

Supersymmetry is a proposed new symmetry that relates bosons and fermions. If supersymmetry is realized in nature, it could provide a solution to the hierarchy problem, and one of the new particles it predicts could explain dark matter. In this thesis, I study supersymmetric models in which the lightest supersymmetric particle can be responsible for dark matter.

I discuss a scenario in which the supersymmetric partner of the top quark called stop is the next-to-lightest supersymmetric particle in the constrained Minimal Supersymmetric Standard Model. Mass limits and various decay branching fractions are considered when the allowed parameter space for the scenario is determined. If the mass of stop is close to the mass of the lightest supersymmetric particle, one can obtain the observed dark matter density. The scenario leads to a novel experimental signature consisting of high transverse momentum top jets and large missing energy, which can be used to probe the model at the LHC.

I also discuss an extended supersymmetric model with spontaneous charge-parity (CP) violation and a right-handed neutrino. When CP is spontaneously violated, a light singlet scalar appears in the particle spectrum, which provides new annihilation channels for the lightest supersymmetric particle. In the model, a neutralino or a right-handed sneutrino can produce the observed dark matter density. Dark matter direct detection limits are found to be especially constraining for right-handed sneutrinos.

# Acknowledgements

This thesis is based on work carried out in the Helsinki Institute of Physics and in the Department of Physics of the University of Helsinki. The work has been funded by the Magnus Ehrnrooth foundation.

I would like to thank my supervisor, Katri Huitu, for her guidance and support, and for the opportunity to work on fascinating research projects. I wish also to thank my other collaborators Priyotosh Bandyopadhyay, Kirtiman Ghosh, Jari Laamanen, Santosh Kumar Rai, and Timo Rüppell for their hard work and interesting discussions, and the pre-examiners of this thesis, Gautam Bhattacharyya and Kristjan Kannike, for their comments.

Finally, I thank my family for providing support and encouragement.

Helsinki, December 2014
*Lasse Leinonen*

# List of Publications

This thesis is based on the following publications:

I. K. Huitu, L. Leinonen, and J. Laamanen,
*Stop as a next-to-lightest supersymmetric particle in constrained MSSM*,
Phys.Rev. **D84** (2011) 075021.

II. K. Ghosh, K. Huitu, J. Laamanen, L. Leinonen,
*Top Quark Jets as a Probe of the Constrained Minimal Supersymmetric Standard Model with a Degenerate Top Squark and Lightest Supersymmetric Particle*,
Phys.Rev.Lett. **110** (2013) 141801.

III. K. Huitu, J. Laamanen, L. Leinonen, S. K. Rai, and T. Ruppell,
*Comparison of neutralino and sneutrino dark matter in a model with spontaneous CP violation*,
JHEP **1211** (2012) 129.

## Author's Contribution

Paper 1: I contributed to the computer code and generated the data sets for the particle spectra and constraints of the model. The results were interpreted and the paper was written jointly by all authors.

Paper 2: I wrote an implementation of the Pythia algorithms used in the analysis of the boosted top jet events. I generated the benchmark points and checked the experimental constraints for them. The results were interpreted jointly by all authors.

Paper 3: I implemented the model and developed the related code for micrOMEGAs together with T.R. The results were interpreted and the paper was written jointly by all authors.

# Contents

# Chapter 1

# Introduction

The Standard Model is a remarkably successful description of the fundamental interactions of particle physics. With the discovery of the Higgs boson at the Large Hadron Collider (LHC) and the resulting confirmation of the Higgs mechanism as the source of electroweak symmetry breaking, this theory of strong and electroweak interactions is established to be in very good agreement with the experimental data. There are, however, several phenomena that are not explained by the Standard Model. For instance, these include neutrino masses, dark matter, and dark energy. Neutrinos are massless in the Standard Model, but the observed flavor oscillations point to massive neutrinos and consequently to the existence of right-handed neutrinos. The extensive evidence of dark matter on astronomical and cosmological scales is another sign that the Standard Model must be extended because it does not feature a viable candidate for dark matter. The origin of dark energy, which is responsible for the accelerating expansion of the universe, is also a mystery. The Standard Model is regarded as a low energy effective theory of some more fundamental theory of physics. It is expected that new physics should manifest itself in particle collisions at an energy scale between the electroweak scale and either the grand unification scale, where the gauge interactions are thought to unify, or the Planck scale, where quantum gravitational effects become important.

The observed mass of the Higgs boson is a hint that some new, beyond the Standard Model physics could appear at the TeV scale, which is probed by the LHC. As the Higgs boson is a scalar particle, its mass squared parameter is subject to quadratically divergent quantum corrections proportional to square of the momentum cut-off. These terms arise, for example, from fermion loops shown in Fig. 1.1. In contrast, the other particles of the Standard Model have at most logarithmic divergences. This is because fermions are protected by the approximate chiral symmetry, and gauge bosons are protected by gauge invariance. The momentum cut-off is interpreted as the energy scale at which new physics becomes important and the Standard Model is no longer valid. If the scale of the cut-off is taken to be the grand unification scale $M_U \sim 10^{16}$ GeV, the Higgs mass parameter receives enormous quantum corrections that


Figure 1.1: Quadratically divergent one-loop quantum corrections to the Higgs boson mass parameter from a fermion loop (left) and from a scalar loop (right).

ought to push the mass to a very large value far above the electroweak scale. Since the gauge boson and fermion masses are directly connected to the vacuum expectation value of the scalar field, which in turn depends on the Higgs mass and the Higgs potential, the scale of the electroweak symmetry breaking and interactions seems to be unnaturally low compared with the assumed very high energy scale of a more fundamental theory. This is called the hierarchy problem. For the $\sim 10^{16}$ GeV cut-off, the cancellation between the Higgs mass parameter and the quantum corrections must be fine-tuned with enormous precision in order to obtain the observed Higgs mass. In the absence of excessive fine-tuning, the cut-off is required to be at a significantly lower energy scale, near one TeV. This suggests that some new physics that can stabilize the Higgs mass will enter at the TeV scale.

Supersymmetry can provide a solution to the hierarchy problem. In supersymmetric theories, bosons and fermions are related in such a way that each fermion field has a bosonic partner. With the relation, cancellation of quadratic divergences is possible since fermion and boson loops in quantum correction diagrams are associated with opposite signs. The quadratically divergent contributions to the squared Higgs mass arising from the loop diagrams in Fig. 1.1 cancel exactly if for each quark and charged lepton there exists two complex scalar partners and the associated dimensionless couplings of the particles are related. Supersymmetry guarantees these conditions. Furthermore, supersymmetry guarantees that all quadratic divergences for squared scalar masses cancel to all orders in perturbation theory. Although this stabilizes the electroweak scale from the quadratic quantum corrections, it does not explain the origin of the scale. However, supersymmetric models can provide an attractive mechanism for breaking the electroweak symmetry. The breaking can be induced radiatively by renormalization effects if a Higgs boson squared mass parameter that is positive at a high energy scale is driven to a negative value at the electroweak scale. This occurs naturally in many models in which the scalar mass parameters at the high energy scale are roughly of order one TeV.

The hierarchy problem indicates that supersymmetry could very well be an essential feature of TeV scale physics. In addition to the stability of the Higgs mass, supersymmetry has also other compelling features. One of them is the apparent unification of the gauge couplings. In the Standard Model, the gauge couplings evolved to a high energy scale with renormalization group equations

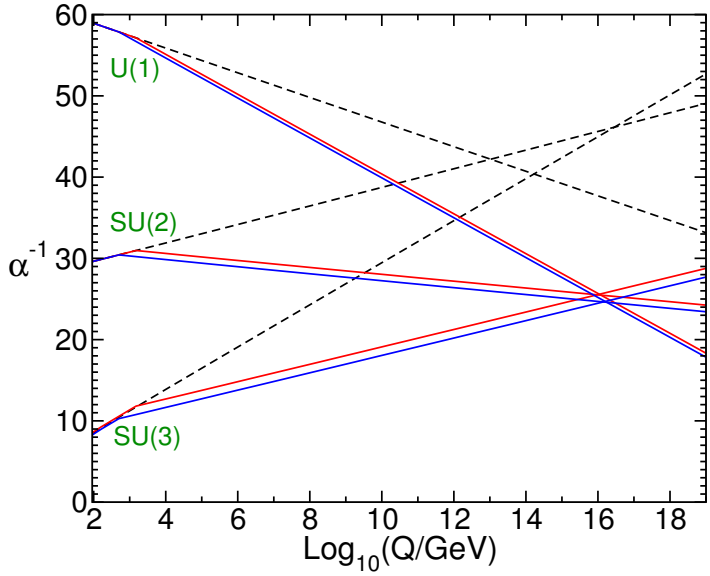


Figure 1.2: Renormalization group evolution of the inverse gauge couplings in the Standard Model (dashed lines) and in the Minimal Supersymmetric Standard Model (solid lines for two different mass scales of supersymmetric particles near one TeV) [1].

do not unify at any point, as seen in Fig. 1.2, whereas the new particle content in the minimal supersymmetric extension of the Standard Model alters the running of the couplings to the extent that the unification can take place at the scale $M_U$. The unification is compatible with supersymmetric particle masses that are within a few orders of magnitude of the TeV scale, which intriguingly is similar to the mass scale suggested by fine-tuning arguments related to the hierarchy problem. The possible unification of the gauge couplings points to a supersymmetric grand unification of strong and electroweak interactions. Remarkably, supersymmetry has also a fundamental connection to gravity. When supersymmetry is treated as a local symmetry, it is a theory of gravity encompassing general relativity.

Another interesting aspect of supersymmetry is that it can provide viable dark matter candidates. The lightest supersymmetric particle is stable if a discrete symmetry called R-parity is conserved. Stable, massive, and neutral supersymmetric particles are often good dark matter candidates. Typically, these dark matter candidates can be produced thermally in the early universe. As thermal relics with electroweak scale interactions, they could naturally explain the observed cold dark matter density. Searches for dark matter have been carried out in both direct and indirect detection experiments. Some of the experiments claim to have seen a possible signal of dark matter, but these signals could be due to background noise from other sources. The most recent

and sensitive direct detection experiments have not observed any new weakly interacting massive particles. This places stringent limits on the cross sections and masses of the dark matter candidates in supersymmetric models.

Searches for the new particles predicted by supersymmetry in collider experiments have been so far without success. It is expected that if supersymmetry is the solution to the hierarchy problem, the mass scale of supersymmetric particles is within the reach of the LHC. While supersymmetry removes the quadratic dependence on the cut-off for the Higgs boson squared mass, in supersymmetric extensions of the Standard Model the Higgs mass parameters are sensitive to the squared masses of supersymmetric particles. Since the Higgs mass parameters determine the scale of the electroweak interactions, the masses of supersymmetric particles cannot be very large without having to resort to fine-tuning of the parameters.

# Chapter 2

# Supersymmetry

Supersymmetry is a symmetry that relates bosons and fermions. Extending the work of Coleman and Mandula [2] on the possible symmetries of relativistic field theories, Haag et al. [3] showed that supersymmetry is the most general extension of the Poincaré algebra. The generator of supersymmetry transformations $Q$, which changes bosons into fermions, and vice versa, is a spinor generator with anticommutation relations. The simplest form for the generator is a two component Weyl spinor $Q_\alpha$ and its Hermitian conjugate. They satisfy the relations

$$[P_\mu, Q_\alpha] = [P_\mu, \overline{Q}_{\dot{\alpha}}] = 0, \tag{2.1}$$

$$\{Q_\alpha, Q_\beta\} = \{\overline{Q}_{\dot{\alpha}}, \overline{Q}_{\dot{\beta}}\} = 0, \tag{2.2}$$

$$\{Q_\alpha, \overline{Q}_{\dot{\gamma}}\} = 2\sigma^\mu_{\alpha\dot{\gamma}} P_\mu, \tag{2.3}$$

where $\sigma^\mu = (1, \sigma^i)$, $P_\mu$ is the momentum operator, and $\sigma^i$ are the Pauli matrices. It is possible to extend the Poincaré algebra with multiple distinct supersymmetry generators, but only the supersymmetric theories with a single spinor generator allow for chiral fermions.

Irreducible representations of supersymmetry are called supermultiplets, which contain both bosons and fermions. In each supermultiplet, there is an equal number of bosonic and fermionic states. Particles in the same supermultiplet are called superpartners of each other. Since $Q_\alpha$ and $\overline{Q}_{\dot{\alpha}}$ commute with $P_\mu$, they also commute with the mass operator $P^2$, so all particles in a supermultiplet have the same mass. There are two important types of supermultiplets in supersymmetric extensions of the Standard Model: chiral supermultiplets, which consist of a Weyl fermion and a complex scalar, and vector supermultiplets, which consist of a gauge boson and a Weyl fermion.

## 2.1 Supersymmetric Theories

Construction of supersymmetric Lagrangians is simplified with the use of superfields. Here, we briefly discuss the main points. A more detailed account can

be found, for example, in [1, 4, 5]. Unlike ordinary fields, which depend only on space-time coordinates, superfields depend on coordinates of superspace. A superfield $S(x, \theta, \bar{\theta})$ is a function of Grassmann variables $\theta_\alpha$, $\bar{\theta}_{\dot{\alpha}}$, and space-time coordinates $x^\mu$. The anticommuting Grassmann variables transform as two-component Weyl spinors:

$$\{\theta_\alpha, \theta_\beta\} = \{\theta_\alpha, \bar{\theta}_{\dot{\beta}}\} = \{\bar{\theta}_{\dot{\alpha}}, \bar{\theta}_{\dot{\beta}}\} = 0. \tag{2.4}$$

A power series expansion of a function in terms of an anticommuting variable is finite since the product of the variable with itself is zero. So the expansion of a superfield $S(x, \theta, \bar{\theta})$ in terms of the two-component Grassmann variables $\theta_\alpha$ and $\bar{\theta}_{\dot{\alpha}}$ has terms involving up to a square of $\theta$ and $\bar{\theta}$.

In superspace formalism supersymmetry generators act on superfields. Supersymmetry algebra and transformations are realized with the generators represented as differential operators. In the linear representation, the generators can be defined as

$$Q_\alpha = i\frac{\partial}{\partial\theta^\alpha} - \sigma^\mu_{\alpha\dot{\alpha}}\bar{\theta}^{\dot{\alpha}}\partial_\mu, \quad \overline{Q}_{\dot{\alpha}} = -i\frac{\partial}{\partial\bar{\theta}^{\dot{\alpha}}} + \theta^\alpha\sigma^\mu_{\alpha\dot{\alpha}}\partial_\mu. \tag{2.5}$$

An infinitesimal supersymmetry transformation parametrized by Grassmann variables $\xi$ and $\bar{\xi}$ is then given by

$$\begin{aligned}\delta_\xi S(x^\mu, \theta, \bar{\theta}) &= -i(\xi Q + \bar{\xi}\overline{Q})S = \left[\xi^\alpha\frac{\partial}{\partial\theta^\alpha} + \bar{\xi}_{\dot{\alpha}}\frac{\partial}{\partial\bar{\theta}_{\dot{\alpha}}} + i(\xi\sigma^\mu\bar{\theta} + \bar{\xi}\bar{\sigma}^\mu\theta)\partial_\mu\right] S \\ &= S(x^\mu + i\xi\sigma^\mu\bar{\theta} + \bar{\xi}\bar{\sigma}^\mu\theta, \xi + \theta, \bar{\xi} + \bar{\theta}) - S(x^\mu, \theta, \bar{\theta}),\end{aligned} \tag{2.6}$$

where repeated spinor indices are suppressed. Irreducible representations can be found by imposing constraints on superfields. Derivatives that are covariant under supersymmetry transformations can be used as constraints and are useful for building supersymmetric Lagrangians. One can define covariant derivatives

$$D_\alpha = \frac{\partial}{\partial\theta^\alpha} - i\sigma^\mu_{\alpha\dot{\alpha}}\bar{\theta}^{\dot{\alpha}}\partial_\mu, \quad \overline{D}^{\dot{\alpha}} = -\frac{\partial}{\partial\bar{\theta}_{\dot{\alpha}}} + i\bar{\sigma}^{\mu\dot{\alpha}\alpha}\theta_\alpha\partial_\mu. \tag{2.7}$$

These operators anticommute with the supersymmetry generators and superspace Grassmann variables, so they commute with the supersymmetry transformation of (2.6).

### 2.1.1 Chiral Superfields

Chiral superfields, which can be used to describe chiral supermultiplets, are defined by imposing covariant constraints on superfields. A left-chiral superfield $\Phi$ satisfies the condition

$$\overline{D}^{\dot{\alpha}}\Phi = 0. \tag{2.8}$$

To solve this, it is useful to define a new variable $y^\mu = x^\mu - i\theta\sigma^\mu\bar{\theta}$. In terms of the variables $y^\mu$, $\theta$, and $\bar{\theta}$, the covariant derivative is

$$\overline{D}^{\dot{\alpha}} = -\frac{\partial}{\partial\bar{\theta}_{\dot{\alpha}}}. \tag{2.9}$$

The left-chiral constraint is now satisfied for any function of $y^\mu$ and $\theta$. $\Phi(y,\theta)$ expanded in powers of $\theta$ is

$$\Phi(y^\mu,\theta) = \phi(y) + \sqrt{2}\,\theta\psi(y) + \theta\theta F(y), \tag{2.10}$$

where the factor $\sqrt{2}$ is chosen by convention. A left-chiral superfield $\Phi$ that describes a chiral supermultiplet consists of a left-handed Weyl spinor field $\psi$, and complex scalar fields $\phi$ and $F$. Under an infinitesimal supersymmetry transformation $\delta_\xi\Phi = -i(\xi Q + \bar{\xi}\overline{Q})\Phi$, the component fields transform as

$$\begin{aligned}\delta\phi &= \sqrt{2}\,\xi\psi,\\ \delta\psi_\alpha &= \sqrt{2}\,\xi_\alpha F - i\sqrt{2}\,\sigma^\mu\bar{\xi}\,\partial_\mu\phi,\\ \delta F &= i\sqrt{2}\partial_\mu\psi\,\sigma^\mu\bar{\xi}.\end{aligned} \tag{2.11}$$

This indicates that the $F$-component (coefficient of $\theta\theta$) of any left-chiral superfield transforms into a total derivative. The set of component fields $\phi$, $\psi$, and $F$ transform into each other. This set cannot be reduced, since the fields left out would appear again after a supersymmetry transformation. Compared with the chiral supermultiplet, the left-chiral superfield has an additional complex scalar field $F$. It is, however, only an auxiliary field whose purpose is to close the supersymmetry algebra linearly off-shell. Without it, there would not be an equal amount of fermionic and bosonic degrees of freedom in the superfield. For a right-chiral superfield $\Phi^\dagger$, the covariant constraint is

$$D_\alpha\Phi^\dagger = 0. \tag{2.12}$$

The component fields of a right-chiral superfield $\Phi^\dagger$ are a right-handed Weyl spinor field $\overline{\psi}$, and complex scalar fields $\phi^\dagger$ and $F^\dagger$.

### 2.1.2 Vector Superfields

To construct supersymmetric gauge theories one also needs vector supermultiplets, which contain real gauge fields and their fermionic superpartners called gauginos. A superfield representation of a vector supermultiplet is found by requiring that a superfield $V$ satisfies the constraint

$$V(x,\theta,\bar{\theta}) = V^\dagger(x,\theta,\bar{\theta}). \tag{2.13}$$

Under this constraint the superfield $V$ is real. Real superfields are referred to as vector superfields. A vector superfield representing a vector multiplet contains a gaugino field $\lambda$, a vector field $A_\mu$, and an auxiliary real scalar field $D$. There are also other auxiliary fields in the vector superfield, but they can be removed by a supersymmetric gauge transformation. The vector superfield is then in the Wess-Zumino gauge, and is given by

$$V_{\mathrm{WZ}} = \theta\sigma^\mu\bar{\theta}A_\mu(x) + \theta\theta\bar{\theta}\bar{\lambda}(x) - \bar{\theta}\bar{\theta}\theta\lambda(x) - \frac{1}{2}\theta\theta\bar{\theta}\bar{\theta}D(x). \tag{2.14}$$

The component field $D$ transforms as

$$\delta D = i\xi\sigma^\mu\partial_\mu\bar{\lambda} + i\bar{\xi}\,\bar{\sigma}^\mu\partial_\mu\lambda, \tag{2.15}$$

which shows that the $D$-component (coefficient of $\bar{\theta}\bar{\theta}\theta\theta$) of any vector superfield transforms into a total derivative.

### 2.1.3 Lagrangians

Supersymmetric Lagrangians are constructed from superfields and their products. Since the $F$-component of a left-chiral superfield and the $D$-component of a vector superfield transform into a total derivative under a supersymmetry transformation, the action $S = \int d^4x$ of these components is invariant under supersymmetry transformations. The $F$- and $D$-terms constructed from superfields of are therefore candidates for a supersymmetric Lagrangian.

One can see from the form of the left-chiral superfields in eq. (2.10) that a product of two left-chiral superfields also satisfies the left-chiral condition (2.8) and therefore is a left-chiral superfield, as is any combination of left-chiral superfields. In a renormalizable theory, the total mass dimension of the fields in each term is four or less. Accordingly, the $F$-term that describes the non-gauge interactions of chiral supermultiplets can consist of products of up to three left-chiral superfields because a scalar field $\phi$ has mass dimension one, a fermion field $\psi$ has mass dimension 3/2, and an auxiliary field $F$ has mass dimension 2. The function of these left-chiral superfields is called the superpotential. One can write a general superpotential as

$$W(\Phi) = L^i\Phi_i + \frac{1}{2}m^{ij}\Phi_i\Phi_j + \frac{1}{3}\lambda^{ijk}\Phi_i\Phi_j\Phi_k, \tag{2.16}$$

where the $L^i$ parameters have mass dimension 2, and the mass terms $m^{ij}$ and the dimensionless couplings $\lambda^{ijk}$ are symmetric. The $F$-term of the superpotential can be expressed as

$$[W(\Phi)]_F = \frac{\partial W(\phi)}{\partial\phi_i}F_i - \frac{1}{2}\frac{\partial^2 W(\phi)}{\partial\phi_i\partial\phi_j}\psi_i\psi_j. \tag{2.17}$$

Here $W(\phi)$ is the superpotential where the left-chiral superfields $\Phi_i$ have been replaced by their scalar field components $\phi_i$, and repeated indices are summed over.

Gauge invariant kinetic terms and gauge interactions of a chiral multiplet in a general gauge theory are given by the $D$-term of a composite vector superfield

$$\begin{aligned}[\Phi^\dagger e^{2gt^aV^a}\Phi]_D = {} & \mathcal{D}^\mu\phi^{i*}\mathcal{D}_\mu\phi_i + i\bar{\psi}^i\bar{\sigma}^\mu\mathcal{D}_\mu\psi_i + F^{*i}F_i \\ & - \sqrt{2}g[(\phi^*t^a\psi)\lambda^a + \bar{\lambda}^a(\bar{\psi}\,t^a\phi)] + g\phi^*t^aD^a\phi,\end{aligned} \tag{2.18}$$

where $t^a$ are the generators of the gauge symmetry group. The covariant derivatives are

$$\mathcal{D}_\mu\phi_i = \partial_\mu\phi_i - igA^a_\mu(t^a\phi)_i, \quad \mathcal{D}_\mu\psi_i = \partial_\mu\psi_i - igA^a_\mu(t^a\psi)_i. \tag{2.19}$$

An irreducible representation that consists of the fields $F^a_{\mu\nu} = \partial_\mu A^a_\nu - \partial_\nu A^a_\mu - g f^{abc} A^b_\mu A^c_\nu$, $\lambda^a$, $\bar{\lambda}^a$, and $D^a$ can be formed from the components of a vector superfield. These fields are the components of the field strength superfield constructed by using covariant derivatives:

$$\mathcal{W}_a = -\frac{1}{4}\overline{D}_{\dot{\alpha}}\overline{D}^{\dot{\alpha}} e^{gt^a V^a} \overline{D}_\alpha e^{gt^a V^a}. \tag{2.20}$$

The field strength superfield is a left-chiral superfield because it satisfies the constraint (2.8). The kinetic terms for the gauge fields and the gauginos are obtained from the gauge invariant $F$-term

$$\frac{1}{4g^2}[\mathcal{W}^{a\alpha}\mathcal{W}_{a\alpha}]_F = -\frac{1}{8}F^{a\mu\nu}F^a_{\mu\nu} - \frac{i}{8}F^{a\mu\nu}\tilde{F}^a_{\mu\nu} + \frac{i}{2}\bar{\lambda}^a\bar{\sigma}^\mu\mathcal{D}_\mu\lambda^a + \frac{1}{4}D^aD^a, \tag{2.21}$$

where $\tilde{F}^a_{\mu\nu} = \frac{1}{2}\epsilon_{\mu\nu\rho\sigma}F^{a\rho\sigma}$, and the covariant derivative is

$$\mathcal{D}_\mu\lambda^a = \partial_\mu\lambda^a + g f^{abc} A^b_\mu \lambda^c. \tag{2.22}$$

The renormalizable supersymmetric Lagrangian is written as

$$\mathcal{L} = \frac{1}{4g^2}([\mathcal{W}^{a\alpha}\mathcal{W}_{a\alpha}]_F + \text{h.c.}) + [\Phi_i^\dagger e^{2g_a t^a V^a}\Phi_i]_D + ([W(\Phi)]_F + \text{h.c.}). \tag{2.23}$$

Now the superpotential must be invariant under the gauge symmetries. The auxiliary fields $F^{i*}$ and $D^a$ have no derivatives in the Lagrangian. They are solved from the equations of motion, which yield

$$F^{i*} = -\frac{\partial W(\phi)}{\partial\phi_i}, \quad D^a = -\sum_i g\phi_i^* t^a \phi_i. \tag{2.24}$$

The tree-level scalar potential is constructed from the auxiliary fields:

$$V = \sum_i \left|\frac{\partial W}{\partial\phi_i}\right|^2 + \frac{1}{2}g^2\sum_a\left(\sum_i \phi_i^* t^a \phi_i\right)^2, \tag{2.25}$$

where the first term is referred to as the $F$-term contribution and the second one as the $D$-term contribution to the potential.

## 2.2 Supersymmetry Breaking

Supersymmetry must be a broken symmetry because otherwise supersymmetric particles would have already been discovered. So if supersymmetry is realized in nature, there must be a mechanism that breaks the symmetry spontaneously in a way that is compatible with the experimental mass limits for supersymmetric particles. It follows from (2.3) that the energy operator can be written as

$$H = P^0 = \frac{1}{4}(Q_1\overline{Q}_{\dot{1}} + \overline{Q}_{\dot{1}}Q_1 + Q_2\overline{Q}_{\dot{2}} + \overline{Q}_{\dot{2}}Q_2). \tag{2.26}$$

Because $H \geq 0$, the vacuum energy $\langle 0|H|0\rangle$ is greater or equal to zero. If the vacuum state is invariant under supersymmetry transformations, then $Q_\alpha|0\rangle = 0$ and $\overline{Q}_{\dot{\alpha}}|0\rangle = 0$, and the vacuum energy vanishes. Conversely, supersymmetry is spontaneously broken and the vacuum energy is positive if there are some fields whose variation is non-zero in the vacuum state. The expectation values of the field variations must not break Lorentz invariance, so the possible terms are the variation of a left-chiral superfield component $\langle 0|\delta\psi|0\rangle = \sqrt{2}\xi\langle 0|F|0\rangle$ or the variation of a vector superfield component $\langle 0|\delta\lambda_\alpha|0\rangle = -i\xi_\alpha\langle 0|D|0\rangle$. Thus the only possibility is that the auxiliary $F$- or $D$-terms acquire non-zero vacuum expectation values. Another way of looking at this is that since the scalar potential is

$$V = \sum_i |F_i|^2 + \frac{1}{2}\sum_a D^a D^a, \tag{2.27}$$

supersymmetry is spontaneously broken if the equations $F_i = 0$ and $D^a = 0$ cannot be simultaneously satisfied.

A general feature of spontaneously broken global symmetries is that a massless Nambu-Goldstone mode arises for each generator of the broken symmetries. For spontaneously broken global supersymmetry, the Nambu-Goldstone particle, called goldstino, is a massless fermion since the supersymmetry generator is fermionic. A new massless fermion is not allowed in light of experimental evidence. However, if supersymmetry is a local symmetry, the goldstino is "eaten" by gravitino, the superpartner of graviton, which then becomes massive. Locally supersymmetric theories involve gravity, so they are referred to as supergravity theories.

Even when global supersymmetry is spontaneously broken, the masses of fermions and bosons at tree-level are still tightly related, which is evident from the mass sum rule. The supertrace of all mass matrices is defined as a weighted sum over squared masses of particles with spin $J$:

$$\mathrm{STr}(\mathcal{M}^2) = \sum_J (-1)^{2J}(2J+1)m_J^2. \tag{2.28}$$

At tree-level, the mass sum rule for scalars, fermions, and vector bosons is

$$\mathrm{STr}(\mathcal{M}^2) = \sum_a g_a \mathrm{Tr}(t^a) D^a. \tag{2.29}$$

The traces of the generators $t^a$ are zero for non-abelian groups, and because the sum of the $U(1)$ charges of a non-anomalous gauge symmetry are zero, the trace also vanishes for the group $U(1)_Y$.

It is difficult to give realistic masses to scalar superpartners of quarks and leptons at tree-level through $F$-term or $D$-term supersymmetry breaking. In the Minimal Supersymmetric Standard Model, there are no gauge singlet superfields, which rules out $F$-term breaking in the model, and $D$-term breaking would introduce vacuum expectation values for some charged scalar fields. Furthermore, the mass sum rule holds for conserved quantities like color charge,

electric charge, and lepton number separately, so even in models where $F$-term breaking is possible, some of the scalar superpartners would too light. One also cannot give masses to gauginos, since there are no scalar-gaugino-gaugino interactions that could generate mass terms when the scalar field obtains a vacuum expectation value. Because of these problems, it is commonly assumed that supersymmetry is spontaneously broken in a hidden sector that does not couple directly to the visible sector supersymmetric particles. Non-renormalizable or loop-level messenger interactions between the two sectors are then responsible for communicating the effects of the breaking to the visible sector.

In fact, there is no definite model of supersymmetry breaking for a realistic supersymmetric extension of the Standard Model. Until we have such a model and know its dynamics, we treat supersymmetric models as effective models that describe the observable consequences of spontaneous breaking of supersymmetry. For this, we need to consider the terms that supersymmetry breaking may induce. The terms should not introduce quadratic divergences to the scalars, so all the couplings should be dimensionful. The general form of the these soft supersymmetry breaking terms [6] in the Lagrangian is given by

$$\begin{aligned}\mathcal{L}_{\text{soft}} = & -\Big(\frac{1}{2}M_\lambda\lambda^a\lambda^a + \frac{1}{6}a^{ijk}\phi_i\phi_j\phi_k + \frac{1}{2}b^{ij}\phi_i\phi_j + t^i\phi_i + \text{h.c.}\Big) \\ & - (m^2)^i_j\phi^{j*}\phi_i - \Big(\frac{1}{2}c_i^{jk}\phi^{*i}\phi_j\phi_k + \text{h.c.}\Big),\end{aligned} \tag{2.30}$$

which includes gaugino masses $M_\lambda$ for each gauge group, scalar couplings $a^{ijk}$ and $c_i^{jk}$, scalar mass terms $b^{ij}$ and $(m^2)^i_j$, and coefficients $t^i$ for tadpole terms. Mass terms for chiral fermions could also be included, but they would be redundant since they can be absorbed into the bilinear terms of the superpotential with a redefinition of the soft scalar masses and couplings. Not all of the soft terms listed above are necessarily allowed. They must respect the given symmetries of the theory; for example, the tadpole term is forbidden if there are no gauge singlet superfields. And if there are gauge singlet superfields, the $c_i^{jk}$ term can cause quadratic divergences to appear. Because the details of supersymmetry breaking are not known, the implications of the breaking are parametrized in effective models by adding all the possible soft terms to the Lagrangian.

The soft terms are dependent on the interactions that connect the visible sector to the supersymmetry breaking hidden sector. Several different models of supersymmetry breaking have been proposed. In the gravity-mediated scenario, there are only gravitational interactions between the sectors. If the $F$ component of a hidden sector superfield acquires a supersymmetry breaking vacuum expectation value $\langle F\rangle$, the soft terms in the visible sector should be of the order of

$$m_{\text{soft}} \sim \frac{\langle F\rangle}{M_P}, \tag{2.31}$$

where $\langle F\rangle$ determines the supersymmetry breaking scale. This scale should be in the range $\sqrt{\langle F\rangle} \sim 10^{10}$ to $10^{11}$ GeV so that we end up with soft terms

in the TeV scale. The mass sum rule in supergravity models is modified by a term proportional to the gravitino mass $m_{3/2} \sim \langle F \rangle / M_P$, which allows us to avoid the problem of the too light scalar masses. In the gauge-mediated supersymmetry breaking scenario, there is a third sector of messenger fields that couple to the hidden sector and have ordinary Standard Model gauge interactions with the visible sector fields. The supersymmetry breaking is transmitted to the messenger sector from the hidden sector, and then from the messenger sector to the visible sector via loop-level gauge interactions, giving soft terms of the order

$$m_{\text{soft}} \sim \frac{g_i^2}{16\pi^2} \frac{\langle F \rangle}{M_{\text{mess}}}, \tag{2.32}$$

where $M_{\text{mess}}$ are the masses of messenger fields. For TeV scale soft masses, the scale of the supersymmetry breaking can be as low as $\sqrt{\langle F \rangle} \sim 10^4$ to $10^5$ GeV. The effects of gravity-mediated breaking should also be present in this scenario, but they can be insignificant in comparison because of the scale of the breaking. There is no problem with the mass sum rule, since it applies only at tree-level.

# Chapter 3

# Minimal Supersymmetric Standard Model

The Minimal Supersymmetric Standard Model (MSSM) is a supersymmetric extension of the Standard Model with the minimal number of fields and couplings such that the model is phenomenologically viable (for reviews, see [1, 7]). The fields of the MSSM are presented in Table 3.1. The vector supermultiplets contain the gauge fields and their gaugino superpartners, while the chiral supermultiplets contain quarks and leptons, and their scalar superpartners, squarks and sleptons. In addition, there are two chiral supermultiplets where the Higgs fields and their supersymmetric partners called higgsinos reside. Whereas the Standard Model has only one Higgs doublet, the MSSM is required to have two. Without a second doublet there would be a gauge anomaly, and also it would not be possible to generate masses for both up-type and down-type quarks since the superpotential is constructed only from left-chiral superfields.

The superpotential of the MSSM is

$$W_{\rm MSSM} = \overline{u}\mathbf{y_u}QH_u - \overline{d}\mathbf{y_d}QH_d, -\overline{e}\mathbf{y_e}LH_d + \mu H_u H_d \tag{3.1}$$

with indices suppressed. For example, the first term with indices restored is $\overline{u}^{ia}(\mathbf{y_u})_i{}^j Q_{ja\alpha}\epsilon^{\alpha\beta}(H_u)_\beta$, where $i$ is a generation index, $a$ is a color index, $\mathbf{y}$ are the Yukawa coupling matrices, and the antisymmetric tensor $\epsilon^{\alpha\beta}$ (with $\epsilon^{12} = 1$) contracts the $SU(2)_L$ terms. The three cubic terms in the superpotential give Yukawa interaction terms to quarks and charged leptons, and to their scalar partners. The only quadratic term in the superpotential is the supersymmetric Higgs mass term.

## 3.1 R-Parity

The terms in the superpotential are chosen such that they are consistent with experimentally observed interactions, but they are not all the possible terms

| | spin 0 | spin 1/2 | spin 1 | $SU(3)_C$ | $SU(2)_L$ | $U(1)_Y$ |
|---|---|---|---|---|---|---|
| $L_i$ | $(\widetilde{\nu}, \widetilde{e}_L)_i$ | $(\nu, e_L)_i$ | | **1** | **2** | $-\frac{1}{2}$ |
| $\overline{e}_i$ | $\widetilde{e}^*_{Ri}$ | $e^\dagger_{Ri}$ | | **1** | **1** | $+1$ |
| $Q_i$ | $(\widetilde{u}_L, \widetilde{d}_L)_i$ | $(u_L, d_L)_i$ | | **3** | **2** | $+\frac{1}{6}$ |
| $\overline{u}_i$ | $\widetilde{u}^*_{Ri}$ | $u^\dagger_{Ri}$ | | $\overline{\mathbf{3}}$ | **1** | $-\frac{2}{3}$ |
| $\overline{d}_i$ | $\widetilde{d}^*_{Ri}$ | $d^\dagger_{Ri}$ | | $\overline{\mathbf{3}}$ | **1** | $+\frac{1}{3}$ |
| $H_u$ | $(H^+_u, H^0_u)$ | $(\widetilde{H}^+_u, \widetilde{H}^0_u)$ | | **1** | **2** | $+\frac{1}{2}$ |
| $H_d$ | $(H^0_d, H^-_d)$ | $(\widetilde{H}^0_d, \widetilde{H}^-_d)$ | | **1** | **2** | $-\frac{1}{2}$ |
| $B$ | | $\widetilde{B}^0$ | $B^0$ | **1** | **1** | 0 |
| $W$ | | $\widetilde{W}^\pm, \widetilde{W}^0$ | $W^\pm, W^0$ | **1** | **3** | 0 |
| $g$ | | $\widetilde{g}$ | $g$ | **8** | **1** | 0 |

Table 3.1: Supermultiplets in the MSSM.

that could be included. In the Standard Model, gauge invariance and renormalizability prohibit couplings that do not conserve lepton and baryon numbers. In supersymmetric models, however, it is possible to have interactions that violate baryon or lepton number yet respect gauge invariance and renormalizability, because one could also include the terms

$$W_{L-\text{violation}} = \frac{1}{2}\lambda_{ijk} L_i L_j \bar{e}_k + \lambda'_{ijk} L_i Q_j \bar{d}_k + \mu_{ri} L_i H_u, \tag{3.2}$$

$$W_{B-\text{violation}} = \frac{1}{2}\lambda''_{ijk} \bar{u}_i \bar{d}_j \bar{d}_k \tag{3.3}$$

in the superpotential. As chiral supermultiplets have the same lepton or baryon number as their constituent particles, the terms in (3.2) violate lepton number by one unit, and the term in (3.3) violates baryon number by one unit. Clearly, these terms can be dangerous since baryon or lepton number violating processes are strongly constrained by experiments. For example, proton decay has not yet been seen, which places very strong limits on the magnitude of either $\lambda'$ or $\lambda''$ coupling.

One can remove the unwanted terms in the superpotential by proposing that there is a new symmetry called R-Parity. R-parity is carried by each particle, and it is defined as

$$P_R = (-1)^{3(B-L)+2s}, \tag{3.4}$$

where $s$ is the spin of the particle. The Standard Model particles including the Higgs bosons have $P_R = +1$, while the new supersymmetric particles have

$P_R = -1$. As a result, if R-parity is conserved in interactions, only the terms in (3.1) are allowed. However, R-parity conservation does not necessarily imply $B$ and $L$ conservation in other, non-minimal supersymmetric models. If R-parity is conserved, supersymmetric particles can be created only in even numbers, and sparticles can decay only to an odd number of lighter sparticles. This has an important consequence: the lightest supersymmetric particle is stable.

## 3.2 Soft Supersymmetry Breaking in the MSSM

The soft supersymmetry breaking terms in the MSSM are

$$\begin{aligned}\mathcal{L}_{\text{soft}}^{\text{MSSM}} = &-\frac{1}{2}\left(M_3\widetilde{g}\widetilde{g} + M_2\widetilde{W}\widetilde{W} + M_1\widetilde{B}\widetilde{B} + \text{h.c}\right) \\ &-\left(\widetilde{\overline{u}}\,\mathbf{a_u}\,\widetilde{Q}H_u - \widetilde{\overline{d}}\,\mathbf{a_d}\,\widetilde{Q}H_d - \widetilde{\overline{e}}\,\mathbf{a_e}\,\widetilde{L}H_d + \text{h.c}\right) \\ &-\widetilde{Q}^\dagger\,\mathbf{m_Q^2}\,\widetilde{Q} - \widetilde{L}^\dagger\,\mathbf{m_L^2}\,\widetilde{L} - \widetilde{\overline{u}}\,\mathbf{m_{\overline{u}}^2}\,\widetilde{\overline{u}}^\dagger - \widetilde{\overline{d}}\,\mathbf{m_{\overline{d}}^2}\,\widetilde{\overline{d}}^\dagger - \widetilde{\overline{e}}\,\mathbf{m_{\overline{e}}^2}\,\widetilde{\overline{e}}^\dagger \\ &-m_{H_u}^2 H_u^* H_u - m_{H_d}^2 H_d^* H_d - (bH_uH_d + \text{h.c.}),\end{aligned} \tag{3.5}$$

with indices suppressed. $M_1$, $M_2$, and $M_3$ are the complex bino, wino, and gluino mass terms. The trilinear scalar couplings $\mathbf{a_u}$, $\mathbf{a_d}$, and $\mathbf{a_e}$ are complex $3 \times 3$ matrices. Since the Lagrangian is real, the $3 \times 3$ matrices for $\mathbf{m_Q^2}$, $\mathbf{m_{\overline{u}}^2}$, $\mathbf{m_{\overline{d}}^2}$, $\mathbf{m_L^2}$, $\mathbf{m_{\overline{e}}^2}$ must be Hermitian. The soft Higgs mass parameters $m_{H_u}^2$ and $m_{H_d}^2$ are real, and the $b$-term can be fixed to be real by redefining the phases of the Higgs fields.

The soft terms can lead to large flavor-changing and CP-violating effects [8, 9]. If the squark and slepton soft squared-mass matrices have off-diagonal components in the same basis as the quark and lepton mass matrices, mixing occurs between different flavors of squarks and and between different flavors of sleptons. In the Standard Model, flavor-changing neutral current (FCNC) processes involving quarks are forbidden at tree-level and are suppressed at loop-level because of the unitarity of the CKM matrix. For example, neutral kaon $K^0$–$\overline{K}^0$ mixing arises from FCNC processes. In the MSSM, there are contributions to kaon mixing from loops involving squarks and gauginos. Squark flavor mixing between the first two generations is strongly constrained by the experimental limit on the kaon $K_L - K_S$ mass difference, which requires that the corresponding off-diagonal terms in the squark soft mass matrices are very small. There are also further restrictions on the squark mass matrices from various particle decays such as $b \to s\gamma$ and other processes. The soft trilinear squark couplings can similarly cause flavor mixing, so their off-diagonal entries are also constrained. In the slepton sector, mixing between different generations leads to violation of lepton number from loop-level processes involving sleptons and gauginos. Lepton number violating decays such as $\mu \to e\gamma$, which are forbidden in the Standard Model, are possible in the MSSM. Experimental limits on lepton number violating decays lead to constraints that require that

the off-diagonal components of the slepton soft mass matrices and the slepton trilinear couplings are small.

In addition to flavor problems with squarks and sleptons, there are also problems with CP-violating effects arising from complex phases of the soft terms, which are constrained by the electric dipole moments of the neutron and the electron. One possible solution for these problems is that the masses of the superpartners are so heavy that their contributions to the FCNC and CP-violating processes are suppressed [10]. Another solution is to assume that the supersymmetry breaking mechanism enforces universality of the soft mass terms,

$$\mathbf{m_Q^2} = m_Q^2\mathbf{1}, \quad \mathbf{m_{\bar{u}}^2} = m_{\bar{u}}^2\mathbf{1}, \quad \mathbf{m_{\bar{d}}^2} = m_{\bar{d}}^2\mathbf{1}, \quad \mathbf{m_L^2} = m_L^2\mathbf{1}, \quad \mathbf{m_{\bar{e}}^2} = m_{\bar{e}}^2\mathbf{1}, \tag{3.6}$$

and that the soft **a**-terms are proportional to the Yukawa matrices,

$$\mathbf{a_u} = A_u\mathbf{y_u}, \quad \mathbf{a_d} = A_d\mathbf{y_d}, \quad \mathbf{a_e} = A_e\mathbf{y_e}, \tag{3.7}$$

and additionally that the soft terms are real. Then the FCNC and CP-violating processes are naturally suppressed. This soft breaking universality is often assumed for convenience in the MSSM because it greatly limits the number of free parameters in the theory.

## 3.3 Electroweak Symmetry Breaking

In the Standard Model, the Higgs mechanism breaks the $SU(3)_C \times SU(2)_L \times U(1)_Y$ gauge symmetry to $SU(3)_C \times U(1)_{EM}$. In order to have realistic model with massive $W^\pm$ and $Z$ gauge bosons, the minimum of the MSSM scalar potential must also spontaneously break the electroweak gauge symmetry. The full scalar potential also includes squark and slepton fields, but we must avoid vacuum expectation values (vevs) for those fields. Vevs for the charged scalar fields would lead to a charge or color breaking minimum, and a vev for a sneutrino field would break R-parity and violate lepton number conservation. This puts constraints on the parameters of the model, though usually the positive mass squared terms for squarks and sleptons can be chosen to be large enough to prevent charge and color breaking from happening. Therefore we can concentrate only on the scalar Higgs potential to study electroweak symmetry breaking.

There are three sources for scalar Higgs field terms in the potential. They are the $F$-term, $D$-term, and the soft supersymmetry breaking term contributions

$$V_F = |\mu|^2|H_u|^2 + |\mu|^2|H_d|^2, \tag{3.8}$$

$$V_D = \frac{1}{2}g'^2(H_u^\dagger Y H_u + H_d^\dagger Y H_d)^2 + \frac{1}{2}g^2\sum_a (H_u^\dagger t^a H_u + H_d^\dagger t^a H_d)^2, \tag{3.9}$$

$$V_{\text{soft}} = m_{H_u}^2|H_u|^2 + m_{H_d}^2|H_d|^2 - (bH_uH_d + \text{h.c.}). \tag{3.10}$$

Putting the terms together, the full Higgs scalar potential can be written as

$$\begin{aligned} V &= (|\mu|^2 + m_{H_u}^2)(|H_u^0|^2 + |H_u^+|^2) + (|\mu|^2 + |m_{H_d}^2|)(|H_d^0|^2 + |H_d^-|^2) \\ &\quad + [b(H_u^+ H_d^- - H_u^0 H_d^0) + \text{h.c.}] \\ &\quad + \frac{1}{8}(g^2 + g'^2)(|H_u^0|^2 + |H_u^+|^2 - |H_d^0|^2 - |H_d^-|^2)^2 \\ &\quad + \frac{1}{2} g^2 |H_u^+ H_d^{0*} + H_u^0 H_d^{-*}|^2. \end{aligned} \tag{3.11}$$

Only the neutral Higgs fields should have vevs. As with charged sleptons and squarks, a vev for a charged Higgs field would break electromagnetism. The vev of one of the Higgs doublets can be rotated with a $SU(2)_L$ gauge transformation to its neutral component, so one can set $H_u^+ = 0$ at the minimum. When $\langle H_u^+ \rangle = 0$, stability requires

$$\frac{\partial V}{\partial H_u^+} = b H_d^- + \frac{1}{2} g^2 H_d^0 H_u^{0*} H_d^- = 0, \tag{3.12}$$

which is non-zero unless $\langle H_d^- \rangle = 0$. Since the charged Higgs fields cannot get vevs, the Higgs scalar potential is safe from electric charge breaking vevs, and we can focus on the potential of neutral scalars.

The neutral scalar potential is

$$\begin{aligned} V =& (|\mu|^2 + m_{H_u}^2)|H_u^0|^2 + (|\mu|^2 + m_{H_d}^2)|H_d^0|^2 - (b\, H_u^0 H_d^0 + \text{h.c.}) \\ &+ \frac{1}{8}(g^2 + g'^2)(|H_u^0|^2 - |H_d^0|^2)^2. \end{aligned} \tag{3.13}$$

The $b$ parameter and the Higgs fields $H_u^0$ and $H_d^0$ can have complex phases. Any phase $b$ may possess can be absorbed by a redefinition of the phase of $H_u^0$ or $H_d^0$, so $b$ can be defined to be real and positive. In addition, since $H_u^0$ and $H_d^0$ have opposite weak hypercharges, their phases can be set to zero with a $U(1)_Y$ gauge transformation. Thus both the $b$ parameter and $H_u^0 H_d^0$ can be made real and positive at the same time. Without loss of generality, $b$ and the vevs can be chosen to be real. This means that it is not possible to have a spontaneous violation of CP in the MSSM from complex vevs at tree-level.

There are two conditions the potential must satisfy. First, the potential should have a stable minimum, that is, it is bounded from below. This condition is met for most of the scalar field values since the positive quartic terms dominate the negative $b$-term. However, there is a direction of field space where the quartic terms disappear. When $H_u^0 = H_d^0$, the potential can have arbitrarily negative value unless

$$2b < 2|\mu|^2 + m_{H_u}^2 + m_{H_d}^2. \tag{3.14}$$

The second condition is that the origin of potential is not a stable minimum, so the determinant of the matrix of second derivatives with respect to $H_u^0$ and $H_d^0$ should be negative. This is true if

$$b^2 > (|\mu|^2 + m_{H_u}^2)(|\mu|^2 + m_{H_d}^2). \tag{3.15}$$

If these two conditions are met, the potential has a stable minimum and the electroweak gauge symmetry is spontaneously broken by the vacuum expectation values of the neutral Higgs fields denoted by $\langle H_u^0 \rangle = v_u$ and $\langle H_d^0 \rangle = v_d$.

After the symmetry breaking, the $W^\pm$ and $Z$ bosons obtain masses. The Higgs gauge kinetic terms yield the gauge boson masses

$$M_Z^2 = \frac{1}{2}(g^2 + g'^2)v^2, \tag{3.16}$$

$$M_W^2 = \frac{1}{2}g^2 v^2, \tag{3.17}$$

where $v = \sqrt{v_u^2 + v_d^2}$. We define the ratio of the vevs as

$$\tan\beta = \frac{v_u}{v_d}. \tag{3.18}$$

Then, at the minimum of the potential

$$\frac{\partial V}{\partial H_u^0} = |\mu|^2 + m_{H_u}^2 - b\cot\beta - (M_Z^2/2)\cos(2\beta) = 0, \tag{3.19}$$

$$\frac{\partial V}{\partial H_d^0} = |\mu|^2 + m_{H_d}^2 - b\tan\beta + (M_Z^2/2)\cos(2\beta) = 0. \tag{3.20}$$

These minimization conditions can be solved for

$$b = \frac{(m_{H_u}^2 + m_{H_d}^2 + 2|\mu|^2)\sin 2\beta}{2}, \tag{3.21}$$

$$|\mu|^2 = \frac{m_{H_d}^2 - m_{H_u}^2\tan^2\beta}{\tan^2\beta - 1} - \frac{1}{2}m_Z^2. \tag{3.22}$$

With the first of these two equations, the parameter $b$ can be expressed in terms of the Higgs mass parameters and the ratio of the vevs. Effectively, $b$ can be traded for $\tan\beta$ as a parameter in the Lagrangian. The second equation connects the value of $|\mu|^2$ to the mass of the $Z$ boson and the soft symmetry breaking masses of the Higgs fields. Similarly to $b$, $|\mu|^2$ can be eliminated in favor of $\tan\beta$ in the Lagrangian, but since only the magnitude of $\mu^2$ is fixed, the phase of $\mu$ (or sign in the case of real valued parameter) remains undetermined.

Even though $\mu$ is not a supersymmetry breaking term, equation (3.22) implies that it should be approximately of the same order as the soft mass parameters. This presents a problem since it is natural to assume that its value as a parameter that respects the symmetries would be associated with the energy scale of some more fundamental theory, and would not be related to the supersymmetry breaking parameters. It may be that the effective value of $\mu$ is generated by supersymmetry breaking or that MSSM needs to be extended in some way. For the phenomenology of MSSM this does not really change things, the equation (3.22) can be used to set the magnitude of $\mu$, even if one cannot completely justify the mass scale of the parameter.

Each of the four scalar Higgs fields is complex valued. In total, there are then eight real degrees of freedom. After the electroweak symmetry is broken, five of those form the mass eigenstates for the neutral $h$, $H$, and $A$, and the charged $H^+$ and $H^-$ Higgs bosons. The three remaining degrees of freedom become the longitudinal modes for the massive $W^\pm$ and $Z$ bosons. Since particles with the same quantum numbers mix, there is mixing in the Higgs sector. Conservation of electric charge forbids mixing between charged and neutral fields, and CP invariance of the Higgs scalar potential does not allow the real and imaginary components of the neutral fields to mix, so there are in total three different mass matrices for the Higgs bosons.

Mass terms for the charged Higgs fields in the Lagrangian are

$$\mathcal{L} \ni \begin{pmatrix} H_u^{+*} & H_d^- \end{pmatrix} \mathbf{m}_{H^\pm}^2 \begin{pmatrix} H_u^+ \\ H_d^{-*} \end{pmatrix}, \tag{3.23}$$

where the mass matrix is

$$\mathbf{m}_{H^\pm}^2 = \begin{pmatrix} \frac{\partial^2 V}{\partial H_u^{+*} \partial H_u^+} & \frac{\partial^2 V}{\partial H_u^{+*} \partial H_d^{-*}} \\ \frac{\partial^2 V}{\partial H_d^- \partial H_u^+} & \frac{\partial^2 V}{\partial H_d^- \partial H_d^{-*}} \end{pmatrix} = \begin{pmatrix} b\cot\beta + M_W^2 c_\beta^2 & b + M_W^2 c_\beta s_\beta \\ b + M_W^2 c_\beta s_\beta & b\tan\beta + M_W^2 s_\beta^2 \end{pmatrix}, \tag{3.24}$$

when the Higgs fields are set to their expectation values after the partial derivatives have been calculated. The angles are defined as $\cos\beta = v_d/v$ and $\sin\beta = v_u/v$. To get the particle masses, we solve the eigenvalues of the mass matrix. They are

$$m_{H^\pm}^2 = b(\frac{v_u}{v_d} + \frac{v_d}{v_u}) + m_W^2 = m_{A^0}^2 + m_W^2, \qquad m_{G^\pm} = 0, \tag{3.25}$$

where an identity for the pseudoscalar Higgs mass squared $m_A^2$ was used, which will come up shortly. The two massless would-be Nambu-Goldstone bosons are eaten by the $W^\pm$ bosons. The mixing matrix for $G^+$ and $H^+$ is given by

$$\begin{pmatrix} G^+ \\ H^+ \end{pmatrix} = \begin{pmatrix} \sin\beta & -\cos\beta \\ \cos\beta & \sin\beta \end{pmatrix} \begin{pmatrix} H_u^+ \\ H_d^{-*} \end{pmatrix}. \tag{3.26}$$

For the neutral Higgs fields, let us first consider the imaginary parts. They have the mass terms

$$\mathcal{L} \ni \frac{1}{2} \begin{pmatrix} \mathrm{Im}H_u^0 & \mathrm{Im}H_d^0 \end{pmatrix} \mathbf{m}_{H_i^0}^2 \begin{pmatrix} \mathrm{Im}H_u^0 \\ \mathrm{Im}H_d^0 \end{pmatrix}, \tag{3.27}$$

with

$$\frac{1}{2}\mathbf{M}_{H_i^0}^2 = \begin{pmatrix} b\cot\beta & b \\ b & b\tan\beta \end{pmatrix}. \tag{3.28}$$

Its eigenvalues are the pseudoscalar Higgs and the would-be Nambu-Goldstone boson masses

$$m_A^2 = b(\frac{v_u}{v_d} + \frac{v_d}{v_u}) = \frac{2b}{\sin 2\beta} = m_{H_u}^2 + m_{H_d}^2 + 2|\mu|^2, \quad m_{G^0} = 0, \tag{3.29}$$

where equation (3.21) was used. The would-be Nambu-Goldstone boson $G^0$ is eaten by the $Z$ boson. The mass eigenstates are given by

$$\begin{pmatrix} G^0 \\ A \end{pmatrix} = \sqrt{2} \begin{pmatrix} \sin\beta & -\cos\beta \\ \cos\beta & \sin\beta \end{pmatrix} \begin{pmatrix} \mathrm{Im}H_u^0 \\ \mathrm{Im}H_d^0 \end{pmatrix}. \tag{3.30}$$

The mass terms of the real components of neutral Higgs fields are

$$\mathcal{L} \ni \frac{1}{2} \begin{pmatrix} \mathrm{Re}H_u^0 & \mathrm{Re}H_d^0 \end{pmatrix} \mathbf{m}_{H_r^0}^2 \begin{pmatrix} \mathrm{Re}H_u^0 \\ \mathrm{Re}H_d^0 \end{pmatrix}, \tag{3.31}$$

and the mass matrix is

$$\frac{1}{2}\mathbf{M}_{H_r^0}^2 = \begin{pmatrix} b\cot\beta + M_Z^2 s_\beta^2 & -b - M_Z^2 c_\beta s_\beta \\ -b - M_Z^2 c_\beta s_\beta & b\tan\beta + M_Z^2 c_\beta^2 \end{pmatrix}, \tag{3.32}$$

whose eigenvalues are the masses of two neutral Higgs bosons $h$ and $H$

$$m_{h,H}^2 = \frac{1}{2}\left[ (m_A^2 + M_Z^2 \pm \sqrt{(m_A^2 + M_Z^2)^2 - 4m_A^2 M_Z^2 \cos^2 2\beta}) \right], \tag{3.33}$$

where $h$ is the lighter one by convention. Their mass eigenstates are given by

$$\begin{pmatrix} h \\ H \end{pmatrix} = \sqrt{2} \begin{pmatrix} \cos\alpha & -\sin\alpha \\ \sin\alpha & \cos\alpha \end{pmatrix} \begin{pmatrix} \mathrm{Re}H_u^0 \\ \mathrm{Re}H_d^0 \end{pmatrix}. \tag{3.34}$$

The mixing angles $\alpha$ and $\beta$ are related with

$$\frac{\sin 2\alpha}{\sin 2\beta} = -\frac{m_{H^0}^2 + m_{h^0}^2}{m_{H^0}^2 - m_{h^0}^2}, \quad \frac{\tan 2\alpha}{\tan 2\beta} = -\frac{m_{A^0}^2 + m_Z^2}{m_{A^0}^2 - m_Z^2}. \tag{3.35}$$

At tree-level, the lightest Higgs boson $h$ mass has an upper limit

$$m_h < m_Z |\cos 2\beta|. \tag{3.36}$$

Radiative corrections to the mass of $h$ are then necessary to reach the observed 125 GeV Higgs boson mass. At one-loop level, the most significant contributions come from top quarks and their supersymmetric partners called stops. In this approximation [11], the mass of the lightest Higgs boson is

$$\begin{aligned} m_h^2 &= m_h^{2,\mathrm{tree}} + \Delta m^{2,\text{1-loop}} \\ &= m_Z^2 \cos^2(2\beta) + \frac{3m_t^4}{4\pi^2 v^2} \left( \ln\frac{m_S^2}{m_t^2} + \frac{X_t^2}{M_S^2}\left(1 - \frac{X_t^2}{12M_S^2}\right)\right), \end{aligned} \tag{3.37}$$

where $M_S$ is the average of the stop masses, and

$$X_t = A_t - \mu \cot \beta \tag{3.38}$$

is the stop mixing parameter, as we will see later. Clearly, in (3.37), there exists a value of $X_t$ which maximizes the expression. The absolute value of the mixing term in that case is $X_t = \sqrt{6} M_S$. This is called the Higgs maximal mixing scenario.

## 3.4 Neutralinos and Charginos

After the electroweak symmetry has been broken, higgsinos and electroweak gauginos with the same quantum numbers mix with each other. Neutral gaugino and higgsino fields $\widetilde{B}$, $\widetilde{W}^0$, $\widetilde{H}_d^0$, and $\widetilde{H}_u^0$ mix to form four mass eigenstates called neutralinos, whereas the charged gaugino fields $\widetilde{W}^+$ and $\widetilde{W}^-$ mix with the charged higgsino fields $\widetilde{H}_u^+$ and $\widetilde{H}_u^-$ forming two mass eigenstates called charginos, both having charges $\pm 1$.

The gaugino-higgsino mixing terms arise from

$$\mathcal{L} \ni -\sqrt{2} g \left(\phi^* t^a \psi\right) \lambda^a + \text{h.c.}, \tag{3.39}$$

when the neutral Higgs fields acquire vevs. The gaugino fields $\lambda^a$ are identified as $\lambda^0 = \widetilde{B}$, $\lambda^3 = \widetilde{W}^0$, $(\lambda^1 - i\lambda^2)/\sqrt{2} = \widetilde{W}^-$, and $(\lambda^1 + i\lambda^2)/\sqrt{2} = \widetilde{W}^+$. The mass terms for the electroweak gauginos in the soft supersymmetry breaking Lagrangian are

$$\mathcal{L} \ni= -\frac{1}{2} M_1 \widetilde{B}\widetilde{B} - \frac{1}{2} M_2 \widetilde{W}\widetilde{W} + \text{h.c.}, \tag{3.40}$$

and the superpotential contributions to the higgsino masses are

$$\mathcal{L} \ni -\mu (\widetilde{H}_u^+ \widetilde{H}_d^- - \widetilde{H}_u^0 \widetilde{H}_d^0) + \text{h.c.} \tag{3.41}$$

First, let us examine the neutralino sector. In the gauge eigenstate basis

$$\psi^0 = (\widetilde{B}, \widetilde{W}^0, \widetilde{H}_d^0, \widetilde{H}_u^0), \tag{3.42}$$

the neutral gaugino and higgsino mass terms can be written as

$$\mathcal{L}_{\text{neutralino}} = -\frac{1}{2} (\psi^0)^T \mathbf{M}_{\widetilde{\chi}^0} \psi^0 + \text{h.c.}, \tag{3.43}$$

with

$$\mathbf{M}_{\widetilde{\chi}^0} = \begin{pmatrix} M_1 & 0 & -g' v_d/\sqrt{2} & g' v_u/\sqrt{2} \\ 0 & M_2 & g v_d/\sqrt{2} & -g v_u/\sqrt{2} \\ -g' v_d/\sqrt{2} & g v_d/\sqrt{2} & 0 & -\mu \\ g' v_u/\sqrt{2} & -g v_u/\sqrt{2} & -\mu & 0 \end{pmatrix}. \tag{3.44}$$

The mass matrix can be diagonalized by using a unitary matrix $N$:

$$\mathbf{N}^* \mathbf{M}_{\widetilde{\chi}^0} \mathbf{N}^{-1} = \mathbf{M}^D_{\widetilde{\chi}^0}, \tag{3.45}$$

where $(\mathbf{M}^D_{\widetilde{\chi}^0})_{ii} = m_{\widetilde{\chi}^0_i}$. Then, the neutralino mass eigenstates are

$$\widetilde{\chi}^0_i = \mathbf{N}_{ij} \psi^0_j = \mathbf{N}_{i1} \widetilde{B} + \mathbf{N}_{i2} \widetilde{W}^0 + \mathbf{N}_{i3} \widetilde{H}^0_d + \mathbf{N}_{i4} \widetilde{H}^0_u, \tag{3.46}$$

which, by convention, are labeled $i = 1, 2, 3, 4$ from lightest to heaviest. The composition of the neutralino states depends mostly on the parameters $M_1$, $M_2$, and $\mu$. If $|\mu| \gg |M_{1,2}|, M_Z$, the two lightest neutralinos are a bino-like $\widetilde{\chi}^0_1 \simeq \widetilde{B}$ and a wino-like $\widetilde{\chi}^0_2 \simeq \widetilde{W}^0$ with masses of about $|M_1|$ and $|M_2|$, while the two heaviest mass eigenstates are higgsino-like $\simeq (\widetilde{H}^0_u \pm \widetilde{H}^0_d)/\sqrt{2}$ with masses of about $|\mu|$. If $|\mu| \ll |M_1|$, the two lightest neutralinos are higgsino-like.

Now we consider the charged gaugino and higgsino fields. In the gauge eigenstate basis

$$\psi^{\pm} = (\widetilde{W}^+, \widetilde{H}^+_u, \widetilde{W}^-, \widetilde{H}^-_d), \tag{3.47}$$

the chargino mass terms are

$$\mathcal{L}_{\text{chargino mass}} = -\frac{1}{2} (\psi^{\pm})^T \mathbf{M}_{\widetilde{\chi}^{\pm}} \psi^{\pm} + \text{h.c.}, \tag{3.48}$$

with

$$\mathbf{M}_{\widetilde{\chi}^{\pm}} = \begin{pmatrix} 0 & \mathbf{X}^T \\ \mathbf{X} & 0 \end{pmatrix}, \tag{3.49}$$

where

$$\mathbf{X} = \begin{pmatrix} M_2 & g v_u \\ g v_d & \mu \end{pmatrix} = \begin{pmatrix} M_2 & \sqrt{2} s_\beta \, M_W \\ \sqrt{2} c_\beta \, M_W & \mu \end{pmatrix}. \tag{3.50}$$

The chargino mass matrix can be diagonalized by a singular value decomposition

$$\mathbf{U}^* \mathbf{X} \mathbf{V}^{-1} = \begin{pmatrix} m_{\widetilde{\chi}^{\pm}_1} & 0 \\ 0 & m_{\widetilde{\chi}^{\pm}_2} \end{pmatrix}. \tag{3.51}$$

The positively and negatively charged chargino mass eigenstates are determined with two different mixing matrices

$$\begin{pmatrix} \widetilde{\chi}^+_1 \\ \widetilde{\chi}^+_2 \end{pmatrix} = \mathbf{V} \begin{pmatrix} \widetilde{W}^+ \\ \widetilde{H}^+_u \end{pmatrix}, \quad \begin{pmatrix} \widetilde{\chi}^-_1 \\ \widetilde{\chi}^-_2 \end{pmatrix} = \mathbf{U} \begin{pmatrix} \widetilde{W}^- \\ \widetilde{H}^-_d \end{pmatrix}. \tag{3.52}$$

The masses of the charginos are given by

$$m^2_{\widetilde{\chi}^\pm_1}, m^2_{\widetilde{\chi}^\pm_2} = \frac{1}{2}\Big[|M_2|^2 + |\mu|^2 + 2M_W^2 \mp \sqrt{(|M_2|^2 + |\mu|^2 + 2M_W^2)^2 - 4|\mu M_2 - M_W^2 \sin 2\beta|^2}\Big]. \quad (3.53)$$

If $|\mu| \gg |M_2|, M_W$, the chargino mass eigenstates are wino-like and higgsino-like with masses approximately equal to $|M_2|$ and $|\mu|$.

## 3.5 Gluinos

The gluino is the superpartner of the gluon. Since the $SU(3)_C$ symmetry is unbroken and the gluino is the only color octet fermion, it does not mix with any other particle in the MSSM. The gluino mass term arises from the soft supersymmetry breaking Lagrangian:

$$\mathcal{L} \ni -\frac{1}{2} M_3 \widetilde{g}\widetilde{g} + \text{h.c.} \quad (3.54)$$

At tree-level, the gluino mass is therefore $m_{\tilde{g}} = |M_3|$.

## 3.6 Squarks and Sleptons

Similarly to neutralinos and charginos, scalar fermions that share quantum numbers can mix with each other. Mixing in the squark and charged slepton sectors can get complicated because there are in general $6 \times 6$ mixing matrices that have to be diagonalized. However, constraints from FCNC processes limit the magnitude of flavor mixing between different generations, so we can simplify the analysis by considering mixing only within each flavor.

There are three sources for the mass terms for squarks and sleptons. We can start by considering the mass terms of the top squarks. Then, because similar analysis applies to other squarks and sleptons, we also understand how to write the mass terms of those particles.

Let us begin with the mass terms arising from the superpotential. The relevant part for stop quarks is

$$W \ni \overline{u}\mathbf{y_u} Q H_u + \mu H_u H_d \ni \bar{t} y_t t H_u^0 - \mu H_u^0 H_d^0, \quad (3.55)$$

which leads to the $F$-term contributions

$$\mathcal{L} \ni -m_t^2 \widetilde{t}_R^* \widetilde{t}_R - m_t^2 \widetilde{t}_L^* \widetilde{t}_L + v\mu y_t \cos\beta \widetilde{t}_L^* \widetilde{t}_R + v\mu^* y_t \sin\beta \widetilde{t}_R^* \widetilde{t}_L. \quad (3.56)$$

As before, mass terms are evaluated at the minimum of the potential, so the Higgs fields are set to their vevs. The latter two terms mix the top squark fields $\widetilde{t}_L$ and $\widetilde{t}_R$. The mass terms for top squarks from the soft supersymmetry-breaking Lagrangian are

$$\begin{aligned}\mathcal{L}^{\text{MSSM}}_{\text{soft}} &\ni -\widetilde{Q}^\dagger \mathbf{m_Q^2} \widetilde{Q} - \widetilde{\overline{u}} \mathbf{m_{\overline{u}}^2} \widetilde{\overline{u}}^\dagger - (\widetilde{\overline{u}} \mathbf{a_u} \widetilde{Q} H_u + \text{h.c.}) \\ &\ni -m^2_{Q_3} \widetilde{t}_L^* \widetilde{t}_L - m^2_{\overline{u}_3} \widetilde{t}_R^* \widetilde{t}_R - v a_t \sin\beta \widetilde{t}_R^* \widetilde{t}_L - v a_t^* \sin\beta \widetilde{t}_L^* \widetilde{t}_R. \end{aligned} \quad (3.57)$$

Here we have bilinear terms as well as mixing terms arising from squark-Higgs couplings when the Higgs fields are replaced by their vevs. Finally, the $D$-term contributions

$$\mathcal{L} \ni \frac{1}{2} g^2 \sum_a \Big( \sum_i \phi_i^* t^a \phi_i \Big)^2 \tag{3.58}$$

for top squark masses arise from $SU(2)_L$ $D$-terms involving the fields $\widetilde{Q}_3$ $H_u$, and $H_d$, and from $U(1)_Y$ $D$-terms involving the fields $\widetilde{t}_L$ and $\widetilde{t}_R$. The weak hypercharge of a field $\phi$ is related to the electric charge and the third component of weak isospin by

$$Y_\phi = Q_\phi - T_{3\phi}. \tag{3.59}$$

Using the identity for the hypercharge terms, the $D$-term contributions for top squarks are written as

$$\mathcal{L} \ni -M_Z^2 \cos 2\beta (T_{3\phi} - Q_\phi \sin^2 \theta_W)(\widetilde{t}_L^* \widetilde{t}_L + \widetilde{t}_R \widetilde{t}_R^*). \tag{3.60}$$

Note that $T_{3\phi}$ is zero for superpartners of right-handed fermions. The D-term contributions can be generalized for all squarks and sleptons by

$$\Delta_\phi = M_Z^2 \cos 2\beta (T_{3\phi} - Q_\phi \sin^2 \theta_W). \tag{3.61}$$

We have now found all the parts of the top squark mass matrix. In the gauge eigenstate basis, the top squark mass terms in the Lagrangian are

$$\mathcal{L}_{\text{stop masses}} = -\begin{pmatrix} \widetilde{t}_L^* & \widetilde{t}_R^* \end{pmatrix} \mathbf{m}_{\tilde{\mathbf{t}}}^{\mathbf{2}} \begin{pmatrix} \widetilde{t}_L \\ \widetilde{t}_R \end{pmatrix}, \tag{3.62}$$

where the mass matrix is given by

$$\mathbf{m}_{\tilde{\mathbf{t}}}^{\mathbf{2}} = \begin{pmatrix} m_{Q_3}^2 + m_t^2 + \Delta_{\widetilde{u}_L} & v(a_t^* \sin\beta - \mu y_t \cos\beta) \\ v(a_t \sin\beta - \mu^* y_t \cos\beta) & m_{\widetilde{u}_3}^2 + m_t^2 + \Delta_{\widetilde{u}_R} \end{pmatrix}. \tag{3.63}$$

The mass eigenstates of the matrix are $\widetilde{t}_1$ and $\widetilde{t}_2$, which are called stops. By convention, the latter is the heavier one. With $a_t = y_t A_t$, the off-diagonal entries can be written as $m_t(A_t - \mu \cot\beta)$ if the parameters are real. These terms can induce significant stop mixing when the $A$-term is large. Large mixing terms reduce the masses of the lighter mass eigenstates.

The mass terms for other squarks and sleptons can be obtained similarly. In the basis $(\widetilde{b}_L,\ \widetilde{b}_R)$ and $(\widetilde{\tau}_L,\ \widetilde{\tau}_R)$, the mass matrices for bottom squarks and tau sleptons are

$$\mathbf{m}_{\tilde{\mathbf{b}}}^{\mathbf{2}} = \begin{pmatrix} m_{Q_3}^2 + m_b^2 + \Delta_{\widetilde{d}_L} & v(a_b^* \cos\beta - \mu y_b \sin\beta) \\ v(a_b \cos\beta - \mu^* y_b \sin\beta) & m_{\widetilde{d}_3}^2 + m_b^2 + \Delta_{\widetilde{d}_R} \end{pmatrix}, \tag{3.64}$$

$$\mathbf{m}^{\mathbf{2}}_{\widetilde{\tau}} = \begin{pmatrix} m^2_{L_3} + m^2_\tau + \Delta_{\widetilde{e}_L} & v(a^*_\tau \cos\beta - \mu y_\tau \sin\beta) \\ v(a_\tau \cos\beta - \mu^* y_\tau \sin\beta) & m^2_{\widetilde{e}_3} + m^2_\tau + \Delta_{\widetilde{e}_R} \end{pmatrix}. \tag{3.65}$$

The mass eigenstates of the matrices are sbottoms $\widetilde{b}_1$ and $\widetilde{b}_2$, and staus $\widetilde{\tau}_1$ and $\widetilde{\tau}_2$. The off-diagonal terms can be written as $m_b(A_b - \mu \tan\beta)$ and $m_\tau(A_\tau - \mu \tan\beta)$. Since the bottom and tau masses are considerably smaller than the top quark mass, the extent of the mixing is largely determined by $\tan\beta$.

For the first and second generation squarks and sleptons the mixing is negligible, so the mass eigenstates correspond closely to the gauge eigenstates with masses given by the diagonal entries in their mass matrices.

## 3.7 Minimal Supergravity Model

A commonly used model to study the MSSM is the Minimal Supergravity Model (mSUGRA), which is also referred to as the constrained MSSM (cMSSM). The model is parametrized by assuming that the soft supersymmetry breaking universality given by

$$\mathbf{m}^{\mathbf{2}}_{\mathbf{Q}} = \mathbf{m}^{\mathbf{2}}_{\overline{\mathbf{u}}} = \mathbf{m}^{\mathbf{2}}_{\mathbf{d}} = \mathbf{m}^{\mathbf{2}}_{\mathbf{L}} = \mathbf{m}^{\mathbf{2}}_{\overline{\mathbf{e}}} = m_0^2 \mathbf{1}, \quad m^2_{H_u} = m^2_{H_d} = m_0^2, \tag{3.66}$$

$$M_1 = M_2 = M_3 = m_{1/2}, \tag{3.67}$$

$$\mathbf{a_u} = A_0 \mathbf{y_u},\ \mathbf{a_d} = A_0 \mathbf{y_d},\ \mathbf{a_e} = A_0 \mathbf{y_e}, \tag{3.68}$$

$$b = B_0 \mu \tag{3.69}$$

holds at the gauge coupling unification scale $M_U \sim 10^{16}$ GeV. These boundary conditions can be obtained from the low energy effective Lagrangian of gravity-mediated supersymmetry breaking scenario by assuming a certain minimal form for the non-renormalizable interactions, albeit at the scale $M_P \sim 10^{18}$ GeV. If the MSSM is the correct description of physics between the weak and the unification scales, which is supported by the apparent gauge coupling unification, parameters defined at the unification scale can be evolved to the observable energy scale using renormalization group (RG) equations. Since we understand less about the physics between the unification scale and the Planck scale, the boundary conditions are set at the unification scale. Corrections to this approximation should be absorbed into redefinitions of the soft terms.

The soft supersymmetry breaking terms related to the Higgs fields are constrained by the electroweak symmetry breaking. With the RG evolution, $m^2_{H_u}$ can be driven to a negative value, which generally induces spontaneous breaking of the symmetry. This mechanism is called radiative electroweak symmetry breaking (REWSB). There is an interesting link between REWSB and the large top quark mass since REWSB occurs naturally with large top quark Yukawa couplings.

With the RESWB condition, one can replace $b$ with $\tan\beta$ in the boundary conditions by using the scalar potential minimization conditions, which also allow one to determine the value of $|\mu|^2$. The parameters of the cMSSM are then

$$m_0,\ m_{1/2},\ A_0,\ \mathrm{sign}(\mu),\ \tan\beta. \tag{3.70}$$

# Chapter 4

# Non-Minimal Supersymmetric Models

## 4.1 NMSSM

We saw earlier how the electroweak symmetry breaking conditions in the MSSM demand that the value of the $\mu$ parameter should be roughly of the same order as the soft supersymmetry breaking terms. Since $\mu$ is not a supersymmetry breaking parameter, it is challenging to explain why it is associated with a low energy scale without resorting to fine-tuning. In gravity-mediated supersymmetry breaking models, the problem can be solved by the Giudice-Masiero mechanism [12], which can generate an effective $\mu$ term of the right order from non-renormalizable interactions if the actual $\mu$ term is forbidden at tree-level by some symmetry. There is another solution for the problem in supersymmetric models with a non-minimal field content. An effective $\mu$-like mass term arises from the coupling of a new gauge singlet superfield $S$ to the Higgs superfields $H_u$ and $H_d$ in the superpotential when the scalar field of $S$ acquires a vev induced by the soft breaking terms.

The Next-to-Minimal Supersymmetric Standard Model (NMSSM) [13] has the field content of the MSSM with an additional gauge singlet left-chiral superfield $S$ corresponding to a chiral supermultiplet called $S$, which contains a scalar component $S$ and a fermion component $\widetilde{S}$. With the new superfield, we have new terms in the superpotential as well as new soft supersymmetry breaking terms. The R-parity conserving superpotential for the general NMSSM is

$$W_{\text{NMSSM}} = W_{\text{MSSM}} + \lambda S H_u H_d + \frac{1}{2}\mu' S^2 + \frac{\kappa}{3} S^3. \tag{4.1}$$

The couplings $\lambda$ and $\kappa$ are dimensionless, and $\mu'$ is a supersymmetric mass term.

The soft supersymmetry breaking Lagrangian is then

$$\mathcal{L}_{\text{soft}}^{\text{NMSSM}} = \mathcal{L}_{\text{soft}}^{\text{MSSM}} - \left(\lambda A_\lambda S H_u H_d - \frac{1}{3}\kappa A_\kappa S^3 + \frac{1}{2} m_{S'}^2 S^2 + \xi^3 S + \text{c.c.}\right) - m_S^2 |S^2|. \tag{4.2}$$

The dimensionful terms in the superpotential and the new soft supersymmetry breaking terms should be of the same scale as the MSSM soft terms so that the vev of the singlet scalar determined by the potential minimization condition is not too large and the effective $\mu$ term $\lambda\langle S\rangle = \lambda s$ is of the sought scale. However, there are still supersymmetric terms in the superpotential, including the actual $\mu$ term, and if the soft terms arise from a hidden sector of a supergravity model, the tadpole coupling $\xi^3$ can become quadratically divergent. The unwanted dimensionful terms can be removed by demanding that the full Lagrangian respects $\mathbb{Z}_3$ discrete symmetry, which multiplies the fields in the chiral supermultiplets by $e^{2\pi i/3}$. Under the symmetry, the dimensionful terms $\mu$, $b$, $\xi^3$ $\mu'$ and $m_{S'}^2$ are not allowed. The name NMSSM often refers to the $\mathbb{Z}_3$ invariant model. If it is an exact symmetry, it is spontaneously broken by the Higgs vevs.

After the electroweak symmetry is broken, a spontaneously broken discrete symmetry leads to creation of domain walls [14], which separate degenerate vacua with regions of higher potential. Domain walls are cosmologically disastrous because they can disturb nucleosynthesis and produce large cosmic microwave background anisotropies. There are a number of ways to avoid domain walls. One approach to do this is to assume that the discrete symmetry is explicitly broken at a high energy scale. If the $\mathbb{Z}_3$ breaking terms in the potential are sufficiently large, domain walls disappear before causing problems. This can be dangerous since the tadpole terms can destabilize the hierarchy between the electroweak scale and the Planck scale by inducing a large singlet vev. If we impose additional symmetries on the non-renormalizable terms such that only a harmless tadpole term is generated radiatively, we can avoid the domain wall problem without destabilizing the hierarchy [15].

The particle spectrum of the NMSSM is different from the MSSM because of the singlet superfield. In the Higgs sector, the real part of the singlet scalar field mixes with the real parts of the two neutral Higgs fields, and the imaginary components mix similarly, so there is a new Higgs scalar and a new Higgs pseudoscalar particle. The singlet scalar field modifies the MSSM tree-level upper bound for the Standard Model like Higgs boson to

$$m_h^2 < m_Z^2 \cos^2(2\beta) + \lambda^2 v^2 \sin^2(2\beta). \tag{4.3}$$

This is one of the attractive features of the NMSSM. While the MSSM parameter space is very constrained because of the discovery of 125 GeV mass for the Higgs boson, the singlet superfield contribution to the scalar potential in the NMSSM helps to lift the mass of the particle, making the experimental bound easier to reach. The coupling $\lambda$ has an upper bound of $\sim 0.8$ because otherwise it could have a Landau pole in the renormalization group running of

the coupling below the unification scale. Since the singlet scalar field does not couple to the gauge bosons, a neutral Higgs boson with a large singlet component could be much lighter than the Standard Model-like Higgs boson and still be consistent with constraints from accelerator searches of Higgs bosons. In the neutralino sector, there is an extra particle since the singlet fermion field, which is called the singlino, mixes with the neutral gauginos and higgsinos. In the basis

$$\psi^0 = (\widetilde{B}, \widetilde{W}^0, \widetilde{H}_d^0, \widetilde{H}_u^0, \widetilde{S}) \tag{4.4}$$

the neutralino mass matrix is

$$\mathbf{M}_{\widetilde{\chi}^0} = \begin{pmatrix} M_1 & 0 & -g'v_d/\sqrt{2} & g'v_u/\sqrt{2} & 0 \\ 0 & M_2 & gv_d/\sqrt{2} & -gv_u/\sqrt{2} & 0 \\ -g'v_d/\sqrt{2} & gv_d/\sqrt{2} & 0 & -\lambda s & -\lambda v_u \\ g'v_u/\sqrt{2} & -gv_u/\sqrt{2} & -\lambda s & 0 & -\lambda v_d \\ 0 & 0 & -\lambda v_u & -\lambda v_d & 2\kappa s \end{pmatrix}. \tag{4.5}$$

The singlino field has no gauge couplings, so the neutralinos with a significant singlino component have much smaller couplings to the Standard Model particles than the MSSM neutralinos. For small values of $\lambda v$ and large values of $\kappa s$, the singlino-like neutralino decouples from the rest of the neutralinos, and the neutralino sector of the NMSSM becomes very similar to that of the MSSM.

Spontaneous breaking of CP symmetry is not possible in the MSSM at tree-level because of the structure of the scalar potential. The same is true in the $\mathbb{Z}_3$ invariant NMSSM. However, if the singlet tadpole term exists and $\kappa$ is non-zero, spontaneous breaking of CP in the Higgs sector is possible at tree-level. Spontaneous CP violation occurs if the neutral Higgs fields and the singlet scalar field acquire complex vevs. Only two of these phases are physical since one of them can be absorbed by field redefinitions. The vevs are then

$$\langle H_u^0 \rangle = v_u, \;\; \langle H_d^0 \rangle = v_d e^{i\phi_2}, \;\; \langle S \rangle = s e^{i\phi_S}, \tag{4.6}$$

The neutral Higgs mass matrix is now a $6 \times 6$ matrix that mixes the scalar and pseudoscalar Higgs fields.

## 4.2 NMSSM with Right-handed Neutrinos

Neutrino oscillations have been observed in solar, atmospheric, reactor and accelerator neutrino experiments [16]. Data from the experiments strongly imply that neutrinos mix and have masses, although the absolute values of the masses are not known. The sum of the active neutrino masses is constrained by the Planck and other cosmological observations [17] to be less than one electronvolt. In the Standard Model, neutrinos are massless since there are

no right-handed neutrinos nor interactions that could generate neutrino mass terms from the vev of the Higgs field. In order to include neutrino masses in supersymmetric models, we need to extend the MSSM. Dirac masses for neutrinos are introduced by adding right-handed neutrino superfields with Yukawa couplings in the superpotential. Right-handed neutrinos can additionally have lepton number violating Majorana mass terms. If the Dirac masses are much smaller than the Majorana masses, the smallness of the left-handed neutrino masses can be explained via a seesaw mechanism [18]. Neutrino and sneutrino mass eigenstates are then mixtures of left- and right-handed fields, but the mixing angles are usually small. Since the right-handed neutrino superfields have only Yukawa couplings, neutrino and sneutrino states that consist mostly of the right-handed fields have diminutive couplings to the $Z$ boson. These right-handed neutrinos are called sterile neutrinos.

Right-handed sneutrinos are interesting in the context of the NMSSM. Majorana mass terms for neutrinos can be generated dynamically from the couplings of the right-handed neutrino superfields $N$ to the singlet superfield $S$ in the superpotential when the scalar singlet field obtains a vev. The R-parity conserving but lepton number violating superpotential of the NMSSM with right-handed neutrino superfields is given by

$$W = W_{\text{NMSSM}} + \mathbf{y_N} L H_u N + \lambda_N S N N. \tag{4.7}$$

In addition to generating the Majorana mass terms, the last term in the superpotential allows right-handed sneutrinos to couple to the scalar singlet field, which leads to right-handed sneutrinos having electroweak scale interactions.

In the neutrino sector, the seesaw mechanism generates two different scales for neutrino masses from the Dirac and Majorana mass terms. The neutrino mass matrix is

$$M_\nu = \begin{pmatrix} 0 & m_D \\ m_D^T & M_N \end{pmatrix}, \tag{4.8}$$

where the Dirac masses $m_D$ are proportional to the neutrino Yukawa couplings $y_N$ and the Higgs vev $v_u$ after the electroweak symmetry is broken, and the Majorana mass terms are $M_N = 2\lambda_N \langle S \rangle$ (with indices suppressed). Since $\langle S \rangle$ is roughly of order of the electroweak scale in order to solve the $\mu$ problem, the Majorana mass terms are also approximately of the same order if $\lambda_N$ is of order one. If the Dirac masses are much smaller than the Majorana masses, the left-handed neutrinos are light with masses

$$m_{\nu_L} \approx \frac{y_N^2 v_u^2}{M_N}, \tag{4.9}$$

and the right-handed neutrinos have masses very close to $M_N$. The neutrino Yukawa couplings are then $\mathcal{O}(\lesssim 10^{-6})$ to satisfy the cosmological bounds on the sum of the active neutrino masses. The mixing angles between the left- and right-handed fields are proportional to the Yukawa couplings, so the mixing is

very small, which causes the neutrino mass eigenstates split into left-handed active neutrinos and right-handed sterile neutrinos.

Similarly, mixing between the left- and right-handed sneutrino fields is suppressed because of the small neutrino Yukawa couplings, so the physical sneutrino states consist almost purely of either left- or right-handed sneutrino fields. These left- and right-handed sneutrinos have substantial differences in how they interact with other fields.

# Chapter 5

# Constraints on Supersymmetric Models

## 5.1 Dark Matter

Astronomical and cosmological evidence strongly implies that most of the matter in the universe does not emit or absorb light at any wavelength. Even though the exact nature of this dark matter is not yet understood, as no discovered particle is able to account for it, convincing evidence of dark matter can be seen at multiple scales from small galaxies to largest structures in the universe [19, 20].

The influence of dark matter is directly observed in the rotation curves of spiral galaxies. Rotation curves describe the radial velocities of visible stars and gas as a function of their distance to the galactic center. If the matter in spiral galaxies consisted predominantly of visible matter, the radial velocities should drop with increasing radius, but the observed rotation curves are quite flat even at large distances from the galactic center. This implies that the luminous form of matter is only a small part of the total galactic mass and that there is a halo of dark matter that extends far beyond the edges of the galaxy, which provides the unseen mass. It is difficult to determine how far the halo extends, therefore one cannot place an upper limit on the amount of dark matter in the galaxy. Nevertheless, rotation curves offer very compelling evidence for dark matter.

On a larger scale, existence of dark matter can be established from clusters of galaxies. Methods for determining the mass of a cluster include measuring the radial velocities of the galaxies and applying virial theorem, mapping the distribution of X-ray emissions, and using gravitational lensing. One of the earliest indications of dark matter was found in the velocity dispersion of galaxies in the Coma cluster, which was observed by Zwicky in 1933. Zwicky inferred from the observations that the visible matter alone in the cluster could not explain the motion of the galaxies, and that most of the mass was, in fact,

unseen. As indicated by general relativity, the space around massive galaxy clusters is curved, which causes the light from background objects to lens around the clusters. Thus the magnitude of the gravitational lensing reveals how mass is distributed in the cluster. Mass estimates of galaxy clusters by these independent methods provide strong evidence that the density of dark matter in the clusters is much larger than the density of luminous matter.

Differing characteristics of luminous and dark matter can be seen in the bullet cluster, which is actually a system of two colliding clusters. Bulk of the luminous matter is in two hot X-ray emitting gas clouds instead of the individual galaxies, and gravitational lensing reveals that most of the total mass in the cluster is dark matter [21]. The gas clouds are interacting in the collision with each other and have created shock waves in the process, while the dark matter is only affected by gravity. This implies that dark matter has quite small interactions with both itself and the ordinary luminous matter.

Big Bang nucleosynthesis places a limit on the baryon density in the universe and therefore also on the density of ordinary matter, which is mostly baryonic by mass and is for that reason referred to as baryonic matter. The total baryon density obtained from nucleosynthesis is only a fraction of the total mass density observed from large-scale structure [22, 23], so the possibility that most of dark matter is just dim, difficult to observe baryonic matter is ruled out. Non-baryonic nature of dark matter is also implied by structure formation in the universe. During the early universe, when the temperatures and densities of particles were very high and baryonic matter was in the form of ionized plasma, the radiation pressure of photons pushed against the gravitational pull of mass and kept primordial baryonic matter density fluctuations from growing denser. Dark matter, in contrast, does not couple to photons, so its density fluctuations could grow denser without resistance from radiation. N-body simulations of large-scale structure show that for the initial density fluctuations of luminous matter to evolve into the form of the observed structure of galaxies and clusters, there had to be a significant amount of dark matter to seed the structure formation. In addition, structure formation tells us that the majority of dark matter must be cold, or non-relativistic, since hot, or relativistic dark matter would damp out small scale density fluctuations and cause largest structures to form first. This top-down scenario is in disagreement with the observation that the most distant and earliest objects in the universe are small structures like galaxies.

The standard cosmological model to describe the universe is the $\Lambda$CDM model [24], where $\Lambda$ signifies the cosmological constant and CDM is abbreviation of cold dark matter. This simple yet successful concordance cosmology model, which is named after two of its dominant constituents, seeks to explain the observed large-scale structure, nucleosynthesis of light elements, the accelerating expansion of the universe, and the structure of the cosmic microwave background (CMB) radiation. The model-dependent cosmological parameters are most precisely determined from the observations of the CMB. Anisotropies of the CMB represent the primordial density fluctuations that eventually developed into the large-scale structure we see today. These have been measured

by the Wilkinson microwave anisotropy probe (WMAP) [25] and more recently by the Planck satellite [17], and the data they have gathered confirm that dark matter is indeed non-baryonic. The Planck measurements combined with data from various other observations indicate that the universe is spatially flat and that the total matter density is $\Omega_m = \rho_m/\rho_c = 0.315 \pm 0.017$, where $\rho_c$ is the critical energy density required for the flat geometry. This leaves the remaining energy density to dark energy, which acts like a cosmological constant. While dark energy is not really understood, it is needed to explain the accelerating expansion of the universe indicated by the redshifts of distant supernovae. According to the results, approximately 18 percent of the total matter is baryonic matter, the rest being dark matter. The physical density is often used when the dark matter density is discussed, and the Planck result with 68% confidence level is

$$\Omega_c h^2 = 0.1187 \pm 0.017, \tag{5.1}$$

where $h$ is the reduced Hubble constant ($H_0 = 100h\,\mathrm{km/s/Mpc}$).

Despite the success of the Standard Model, it cannot explain dark matter. In the Standard Model, neutrinos fit the description of non-baryonic particles that interact weakly. Furthermore, the observed flavor oscillations demonstrate that they are massive. Neutrinos, however, are too light to be cold dark matter or to contribute to dark matter density sufficiently. On the other hand, massive neutrinos hint that right-handed sterile neutrinos could exist. If they do, it is possible that they are heavy enough to be warm, or nearly relativistic dark matter, a form of dark matter that is also compatible with structure formation, and to provide the observed non-baryonic matter density. Sterile neutrino dark matter can be produced by different mechanisms, and in some scenarios even relatively cold dark matter can be created [26].

### Dark Matter in Supersymmetric Models

One of the appealing features of supersymmetry is that it can provide a number of viable dark matter candidates. If R-parity is conserved, the lightest supersymmetric particle (LSP) is stable. This implies that an abundance of LSPs remaining from the early universe could account for the dark matter density. Even if supersymmetry is realized in nature, dark matter could have a non-supersymmetric origin, so if a supersymmetric model fails to saturate the density with relic LSPs, it does not necessarily mean that the model is ruled out. While this is the case, it would certainly be nice to be able to explain dark matter in the context of supersymmetry. The upper limit on the cold dark matter density severely constraints the parameter spaces of supersymmetric models such as the MSSM and the NMSSM. The relic density in these models often ends up too high unless the LSPs can annihilate efficiently into Standard Model particles.

Dark matter particles produced thermally in the hot early universe are referred to as thermal relics. Supersymmetric dark matter candidates usually fall

into this category. Initially, in the hot particle soup, a thermal relic is in thermal equilibrium. The equilibrium is maintained as long as the rate of creation and annihilation of the relics is faster than the expansion rate of the universe. When the temperature in the expanding and cooling universe drops below the thermal relic mass, the equilibrium density of the relic becomes suppressed by a Boltzmann factor $\mathrm{e}^{-m/T}$. The relic abundance diminishes exponentially until the expansion rate of the universe is faster than the annihilation rate of the diluted particles. At that point, the relic density is low enough that the particles are unlikely to annihilate each other, so from then on the relic density is no longer determined by the equilibrium density. As the annihilations have mostly ceased, the relic abundance is essentially "frozen out". Their number density is then diluted only by the expansion of the universe.

In a simplified picture, the evolution of the thermal relic number density is described by the Boltzmann equation

$$\frac{dn}{dt} = -3Hn - \langle\sigma v\rangle\,(n^2 - n_{\mathrm{eq}}^2), \tag{5.2}$$

where $H$ is the Hubble expansion rate, $\langle\sigma v\rangle$ is the thermally averaged cross section of the thermal relic annihilation into other particles multiplied by the relative velocity of the relics, and $n_{\mathrm{eq}}$ is the number density in thermal equilibrium. On the right-hand side of the equation, the first term represents the change in the density due to the expansion of the universe and the second term accounts for the creation and annihilation of the relics. Roughly, the equation gives a relic density

$$\Omega_r h^2 \approx 3 \times 10^{-27}\,\mathrm{cm}^3\,\mathrm{s}^{-1}\langle\sigma v\rangle^{-1} \tag{5.3}$$

at present time. The annihilation cross section and the relic density are inversely related. This is because larger cross sections lead to the freeze out taking place later, so the dark matter particle remains longer in the equilibrium, and the density is consequently suppressed further by a smaller Boltzmann factor. It turns out that stable massive particles with weak scale interactions, whose cross section can be estimated as $\langle\sigma v\rangle \sim \alpha^2/(100\,\mathrm{GeV})^2 \sim 10^{-25}\mathrm{cm}^3\mathrm{s}^{-1}$, have naturally relic density close to the right order of magnitude. Whether this is coincidence or not, it lends credence to the idea that a weakly interacting thermal relic could be the most plausible candidate for dark matter. For determining the resulting relic density more accurately, the Boltzmann equation should additionally account for the effect of coannihilations [27]. Coannihilations in supersymmetric models are annihilations between the LSP and other sparticles close to its mass. These can be quite effective in reducing the relic density that otherwise would be too large. To obtain precise results, the calculation of the relic density is usually done numerically.

In the models considered here, the neutral and stable supersymmetric dark matter candidates are the lightest neutralino, the lightest sneutrino, and the gravitino. A bino-like neutralino is often the LSP in the constrained MSSM [28]. Neutralino dark matter tends to be overproduced in supersymmetric models unless the particle spectrum allows an efficient way to annihilate the

particles in the early universe. This is possible to realize, for example, with coannihilations between neutralinos and other sparticles, with a large annihilation cross section through a Higgs resonance (if the neutralino LSP happens to have a mass close to a half of the resonance mass), or with a significant Higgsino mixture in the neutralino allowing it to have an enhanced annihilation rate to the charged gauge bosons. Superpartners of the left-handed neutrinos as the dark matter are excluded by direct detection experiments and collider searches because of their large coupling to the $Z$ boson. Right-handed sneutrinos in the extended models, however, could account for the dark matter. Although gravitino LSP could be the dark matter, the particle would be nearly impossible to detect in experiments. The gravitino mass in gravity-mediated supersymmetry breaking models is similar to the soft breaking masses of other sparticles, whereas the gravitino mass in gauge-mediated models is typically much smaller than the soft breaking scale and, as a result, the gravitino is often the LSP.

## Detection of Dark Matter

Earth is continuously moving through the halo of dark matter in our galaxy. Given the implied energy density of dark matter, dark matter particles should be present in large quantities. If this is the case, some of them are bound to interact with ordinary nuclei even if their scattering cross section with baryonic matter is small. Direct detection experiments aim to observe the interactions of dark matter particles with the target material in the detector. This is done by measuring the recoil energies in elastic scattering events of dark matter with the protons and neutrons in the target material. The event rate is expected to be small, which necessitates a large volume of detector material to capture the signal. It is a challenge to separate signal events from background events, which arise from cosmic rays and radioactivity. This requires careful detector design and analysis of the results in order to avoid false positive signals. Weakly interacting thermal relics with masses from GeV to TeV scale are the prime targets for these searches.

The rate of recoil events depends on the dark matter-nucleon cross section, and the local density and velocity distributions of dark matter. Some halo model, such as the isothermal sphere model, which is simple and is often used in direct detection simulations and analysis, is assumed for the density. For the isothermal model, the corresponding velocity distribution is Maxwellian with an estimated local dark matter density $\rho = 0.3\,\mathrm{GeV/cm^3}$ and a mean velocity $v_0 = 220\,\mathrm{km/s}$. One of the expected experimental signals of a direct detection of dark matter is an annual modulation of the event rate. The modulation should occur because the Earth's motion around the Sun has a seasonal effect on Earth's velocity through dark matter. In addition, the direction of the nucleon recoils should modulate as Earth rotates around its axis.

Results of direct detection experiments are summarized in Figure 5.1. The observations of the DAMA/LIBRA [30], CRESST-II [31], CDMS II [32], and CoGeNT [33, 34] experiments are consistent with a signal of $\sim$10 GeV weakly interacting dark matter particle. DAMA/LIBRA and CoGeNT independently

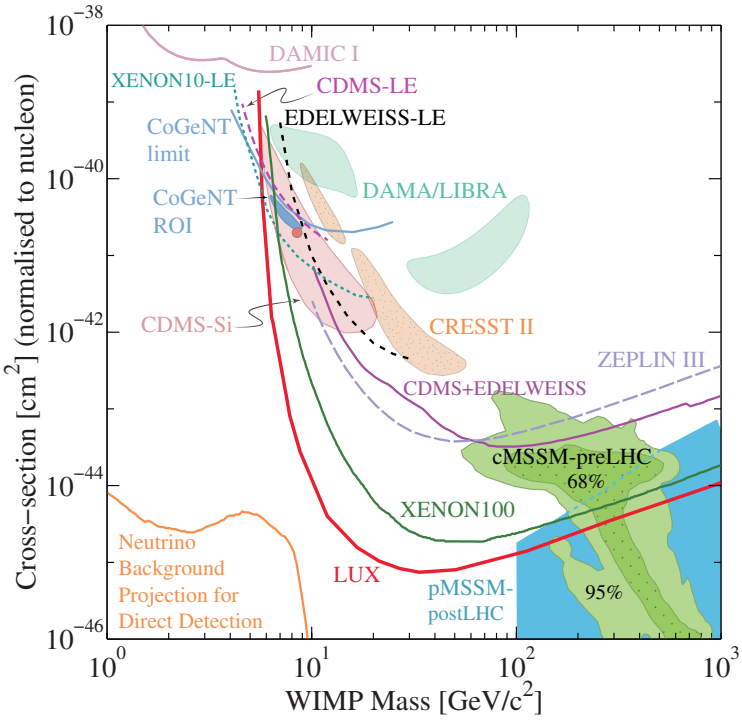


Figure 5.1: Results of direct detections experiments. Exclusion limits and possible signal regions for the spin-independent elastic scattering cross sections and masses of weakly interacting massive particles (WIMPs) [29].

report seeing annual modulation in the event rate, although the statistical significance of the CoGeNT result is only a $2.2\sigma$. The observations of the phase and period of the modulation in the two experiments are compatible with each other and also with halo simulations. The amplitude of the modulation seen by CoGeNT, however, is larger than what is expected for a dark matter halo with a Maxwellian velocity distribution. If the modulation is real, the discrepancy could be due to non-Maxwellian properties of the actual velocity distribution. In contrast to the DAMA/LIBRA and COGeNT results, the CDMS-II experiment, which employs the same target material as CoGeNT, does not find any evidence of annual modulation [35]. The apparent signal of light dark matter in some of the experiments is in disagreement with the results of the xenon-based experiments XENON100 [36] and LUX [37]. These observations put the most stringent limits yet on the spin-independent elastic scattering cross-sections of dark matter particles. It is not known for certain at this point, though, whether the conflict between the experiments is due to background and detector effects erroneously interpreted as signals of dark matter or a possibly lower than assumed sensitivity to low mass dark matter particles in LUX and XENON100.

Indirect detection experiments attempt to detect the annihilation products of dark matter particles. If the dark matter particles are thermal relics with weak interactions, they are predicted to annihilate into particles that include gamma rays, cosmic rays of energetic positrons and electrons, and neutrinos.

Gamma rays from the galactic center are a particularly interesting probe of dark matter annihilations. The dense galactic center is the most promising location to look for the photons because the annihilation rate and consequently the flux of the resulting particles is proportional to the square of the dark matter density. As photons are not charged, they are not deflected by magnetic fields and, as a result, can propagate relatively freely. Consequently, the angular distribution of the observed gamma rays can be used to infer whether their source is consistent with the expected distribution of dark matter. The signature of dark matter annihilating into photons are gamma rays with a specific energy, whereas gamma rays from conventional astrophysical sources are expected to have a continuous spectrum. Searches of excess gamma rays over the galactic background have been carried out by the Fermi Gamma Ray Space Telescope. An independent analysis of the Fermi data points to a signature of dark matter annihilating into $\sim$130 GeV photons [38]. This tentative signal was also found by the Fermi-LAT collaboration using a larger set of data, albeit at a lower statistical significance [39]. Another recent analysis of the Fermi data indicates gamma-ray excess from annihilations of $\sim$30 GeV dark matter particles [40]. The astrophysical background, however, is not perfectly understood. If the background is not estimated properly, gamma rays from ordinary astrophysical sources can be easily misinterpreted as a sign of dark matter.

Annihilation of dark matter in the galactic halo could also lead to an observable excess of positrons. Positrons of astrophysical origin are thought to be created mainly in secondary production from collisions of cosmic ray nuclei with interstellar matter. The flux of positrons measured as a fraction to the rate of incoming cosmic ray electrons is expected to fall with increasing energy. If the dark matter particles annihilate into positrons and electrons either directly or through heavier particles such as the $W$ bosons, the positron fraction should increase at higher energies below the mass of the dark matter particle. The PAMELA experiment has observed a rise in the positron fraction [41], and the Fermi [42] and AMS-02 [43] experiments have later confirmed the results. Even though the rise is intriguing, it does not necessarily mean that dark matter is behind the excess. For one thing, the cross section of the dark matter annihilation required to explain the signal seems to be too large for a thermal relic. A conventional source for the excess positrons could be the magnetospheres of pulsars [44].

High-energy neutrinos from the Sun is another possible signature to look for in indirect detection searches since thermal relic dark matter can accumulate inside massive objects. The accumulation of dark matter inside the Sun relies on small but non-vanishing interactions between dark matter and ordinary matter. A dark matter particle traveling through a celestial body has a small chance of elastically scattering with the nuclei in the matter, and if the

velocity of the particle after scattering is less than it would take it to escape the local gravitational well, the particle becomes trapped and is likely to have further interactions with the body. This causes dark matter particles to lose kinetic energy and sink into the core, where they can annihilate into Standard Model particles. Their decays then give rise to high-energy neutrinos, which are distinctive from the background that mostly consists of atmospheric neutrinos. Dark matter induced neutrinos coming from the sun have been searched in many experiments, including the ANTARES [45], IceCube [46, 47], and Super-Kamiokande [48] neutrino telescopes, but no significant excess above the expected background has been found. These experiments are not as sensitive as the direct detection searches to spin-independent dark matter-nucleon cross sections, but the limits they give on spin-dependent cross sections are more constraining if the main annihilation channel of dark matter particles is to $W^+W^-$ or $\tau^+\tau^-$.

## 5.2 Collider Searches of Supersymmetric Particles

The ATLAS and CMS experiments at the Large Hadron Collider (LHC) at CERN reached one of their primary goals in 2012 with the discovery of the Higgs boson [49, 50]. While the first run of the LHC concluded successfully in 2013, there was unfortunately no sign of supersymmetric particles or conclusive evidence of other new, beyond the Standard Model physics. Nevertheless, the collected data can be used to determine whether a supersymmetric model is still consistent with all the experimental evidence or is ruled out. In searches of new physics it is crucial to understand what are the expected signals of a model with new particles and interactions, and how the signals could be identified from the collider data.

If the mass scale of supersymmetric particles is not too far beyond one TeV, at least some of them should be produced copiously at the LHC. The production of squarks and gluinos, which are strongly interacting, is expected to be dominant over the production of electroweak neutralinos and charginos [51]. The production cross sections, however, are highly dependent on the masses of the sparticles, so the model dependent mass spectrum is a considerable factor in the relative production rate of different sparticles. One important aspect of the colored scalars in the collider phenomenology is that the production rate of the third generation squarks, stops and sbottoms, is smaller than the rate of the first generation of similar masses. The reason for this is that the contributions of the quark scattering processes to the pair production of third generation squarks is negligible because there are virtually no top or bottom quarks in the colliding proton beams.

Supersymmetric particles created in the collisions are expected to decay in cascades, producing a lighter sparticle and Standard Model particles at each step of the decay. If R-parity is conserved, the decay chain continues until there is a final state that contains the stable LSP. Since squarks and gluinos

have color charges, their decays produce strongly interacting Standard Model particles, which undergo hadronization and produce jets of observable particles. Neutralinos and charginos, which are generally expected to be lighter than the colored sparticles, typically produce leptons and jets in their decay chains. The possible decay channels of a supersymmetric particle are determined by the mass spectrum, so the specific experimental signature is dependent on the parameters of the model. But there are some features that are thought to be common in many decays. For squarks and gluinos, the signature of the decay is expected to include one or more high transverse momentum $p_T$ jets from the hadronizations in the cascade and missing energy $\not{E}_T$ from the neutral LSP that escapes the detector. In addition, if there are neutralinos or charginos in the cascade, they can give rise to a signature containing multiple leptons.

In searches of supersymmetry at the LHC, it is often challenging to distinguish the signal from the background produced by ordinary Standard Model processes. Because of this, search strategies have to employ cuts in the event selection to control the background. The cuts determine whether a collision event is considered as a possible signal based on, for example, the amount of missing energy, the number of jets and their transverse momenta in the event. In addition, the cuts can require the events to have a certain number of leptons, and jets originating from the hadronization of top and bottom quarks. Top and bottom jets are usually tagged with jet algorithms that try to identify the origin of the particles in a jet. The LSP is not the only source of missing energy, because neutrinos are also invisible to the detector and carry away energy with them. Furthermore, missing energy also arises from the mismeasurement of jet energies in the detector calorimeters.

In Fig. 5.2 the results of search with the ATLAS detector for pair produced stop squarks are presented for three decay channels. The analysis is carried out with the assumption that stop decays exclusively into one of the decay channels with 100% branching fraction. The mass hierarchy of the supersymmetric particles determines which of the decays are possible. Results of a search for squarks and gluinos with the ATLAS detector detailed in [52] are interpreted in term of the cMSSM in Fig. 5.3. Summaries of the results of searches for supersymmetry at CMS and ATLAS are found in [53, 54]. The results indicate that gluinos and the first two generation squarks are heavier than one TeV. The masses of third generation squarks, charginos, neutralinos, and sleptons can be significantly smaller because they have smaller production cross sections.

## 5.3 Indirect Searches of Supersymmetric Particles

### The $B \to \tau\nu$ Decay

The decay of $B^{\pm}$ mesons to the purely leptonic final states $\tau^{\pm}\,\nu_{\tau}$ are of interest in testing the Standard Model and probing the effects of beyond the Standard Model physics. In the Standard Model, the decay is mediated by a virtual $W$

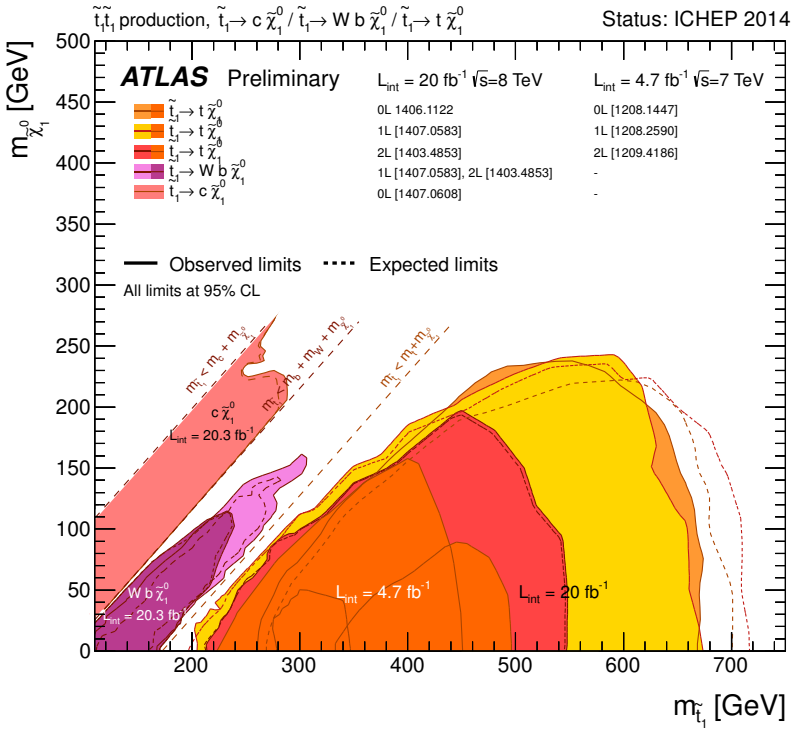


Figure 5.2: Summary of the dedicated ATLAS searches for stop pair production. Exclusion limits are shown in the $\widetilde{t}_1 - \widetilde{\chi}_1^0$ mass plane. The decay modes are considered separately with 100% branching fractions.

boson, and the branching fraction at tree-level is given by

$$\mathcal{B}(B^+ \to \tau^+ \nu_\tau) = \frac{G_F^2 m_B m_\tau^2}{8\pi} \left[1 - \frac{m_\tau^2}{m_B^2}\right] f_B^2 |V_{ub}|^2 \tau_{B^+}, \tag{5.4}$$

where $G_F$ is the Fermi constant, $f_B$ is the $B$ meson decay constant, $|V_{ub}|$ is the absolute value of the CKM matrix element, and $\tau_{B^+}$ is the $B^+$ lifetime. Most of the uncertainty in the prediction lies in the determination of the CKM matrix element. Using the measurement of $|V_{ub}|$ from charmless semileptonic $B$ exclusive decays by the BABAR experiment and the lattice QCD calculation of the decay constant $f_B = 189 \pm 4$ MeV, the value is predicted to be [55]

$$\mathcal{B}(B^+ \to \tau^+ \nu_\tau)_{\mathrm{SM}} = (1.18 \pm 0.16) \times 10^{-4}. \tag{5.5}$$

The branching fraction has been measured in the BABAR [55] and Belle [56] experiments. The BABAR result is

$$\mathcal{B}(B^+ \to \tau^+ \nu_\tau)_{\mathrm{exp}} = (1.79 \pm 0.48) \times 10^{-4}, \tag{5.6}$$

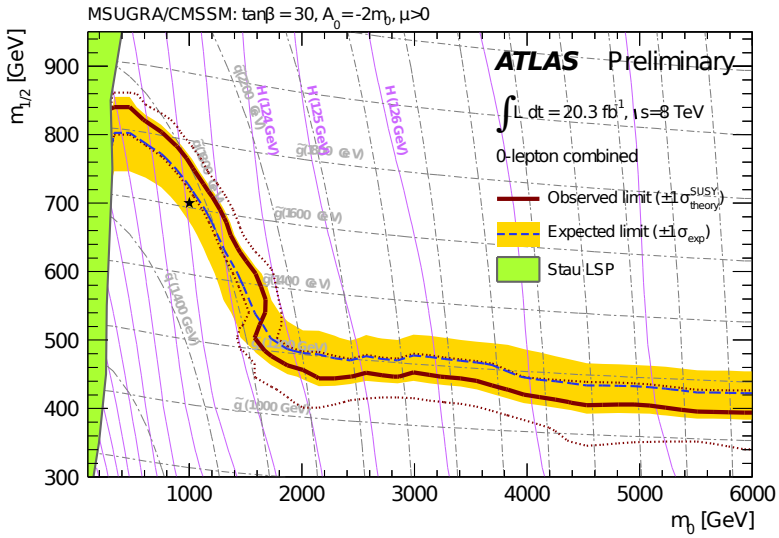


Figure 5.3: ATLAS exclusion limits for cMSSM models with $\tan\beta = 30$, $A_0 = -2m_0$, and $\mu > 0$ in the $m_0 - m_{1/2}$ plane.

while the Belle measurement gives

$$\mathcal{B}(B^- \to \tau^- \nu_\tau)_{\text{exp}} = (0.96 \pm 0.26) \times 10^{-4}. \tag{5.7}$$

There is a small discrepancy between these results. Whereas the branching fraction reported by BABAR exceeds the Standard Model expectation slightly, the Belle result is consistent with the expectation. The branching fraction is sensitive to models with an extended Higgs sector because the decay of $B^\pm$ at tree-level can also be mediated by annihilation into a virtual charged Higgs boson $H^\pm$. The supersymmetric branching fraction [57] is given by

$$\mathcal{B}(B^+ \to \tau^+ \nu_\tau) = \mathcal{B}(B^+ \to \tau^+ \nu_\tau)_{\text{SM}} \times r_H, \tag{5.8}$$

in which $r_H$ that scales the Standard Model rate is

$$r_H = \left(1 - \frac{\tan^2\beta}{1 + \tilde{\epsilon}_0 \tan\beta} \frac{m_B^2}{M_{H^\pm}^2}\right)^2. \tag{5.9}$$

The charged Higgs bosons typically interfere with the $W$ bosons destructively. Higher order corrections to the couplings of charged Higgses to quarks are expressed in $r_H$ by the factor $1/(1 + \tilde{\epsilon}_0 \tan\beta)$, which can be important for large $\tan\beta$. Since the branching fraction depends strongly on the $\tan\beta$ and $M_{H^\pm}$, it can be used as a constraint on those parameters. In supersymmetric models, the constraint typically favors a low $\tan\beta$ or a high $M_{H^\pm}$ in order not to decrease the branching fraction too much below the Standard Model value.

### The $B \to X_s\gamma$ Decay

In the Standard Model, the hadronic process $B \to X_s\gamma$ of the underlying decay $b \to s\gamma$ is a loop-level process, where the most significant lowest order contribution comes from a top-$W$ boson loop. The prediction of the branching fraction at NNLO (next-to-next leading order) is [58]

$$\mathcal{B}(B \to X_s\gamma)_{\mathrm{SM}} = (3.15 \pm 0.23) \times 10^{-4}. \tag{5.10}$$

The present experimental value by the Heavy Flavor Averaging Group [59] together with the BABAR measurement [60] gives the world average of the experimental values [61]

$$\mathcal{B}(B \to X_s\gamma)_{\mathrm{exp}} = (3.43 \pm 0.22) \times 10^{-4}, \tag{5.11}$$

which is consistent with the predicted value. The branching fraction is sensitive to supersymmetric particles and can be used as a constraint for supersymmetric models. Supersymmetric contributions to the decay amplitude come from charged Higgs-top, neutral Higgs-bottom, squark-higgsino, and squark-gaugino loops. In the MSSM and NMSSM, the $b \to s\gamma$ constraint is sensitive to the parameters $\tan\beta$ and $A_t$ [62]. At high $\tan\beta$, large values of $A_t$ increase or decrease the branching fraction significantly depending on the sign of the trilinear term. For a heavy charged Higgs and degenerate squark masses, the parameter space is not really constrained beyond experimental squark mass bounds [61]. If the third generation squarks are light compared with the first two generations of squarks and $A_t$ is negative, the constraint can become relevant even for heavy squark masses. For positive values of $A_t$, the experimental bound is less constraining because the gluino and Higgsino loops partially cancel.

### The $B_s \to \mu^+\mu^-$ branching fraction

The $B_s \to \mu^+\mu^-$ decay is a flavor changing neutral current process, so it can only occur at loop-level. As the decay is also helicity suppressed by the small muon mass, the predicted Standard Model rate is very small. The $B_s \to \mu^+\mu^-$ decay is a good constraint for new physics since the new physics contributions may not be helicity suppressed to the same extent. In the Standard Model, the decay proceeds via penguin and box diagrams, but because of the $B_s^0$–$\bar{B}_s^0$ oscillations, the theoretical branching fraction calculation is not directly comparable with the experimental measurements. Taking into account the different widths between the $B_s$ mass eigenstates, the adjusted prediction is [63]

$$\mathcal{B}(B_s \to \mu^+\mu^-)_{SM} = 3.56 \pm 0.18 \times 10^{-9}, \tag{5.12}$$

which can be compared with the experimental results. Recently, the CMS [64] and LHCb [65] experiments have observed the decay, and the combined result [66] for the branching fraction is

$$\mathcal{B}(B_s \to \mu^+\mu^-)_{\mathrm{exp}} = (2.9 \pm 0.7) \times 10^{-9}. \tag{5.13}$$

This value is in good agreement with the prediction, and does not leave very much room for new physics. In supersymmetric models, the decay amplitude is dominated by Higgs pseudoscalar and heavy Higgs scalar penguin diagrams. The branching fraction receives large enhancement from $\tan\beta$, which strongly constrains the parameter space at large values of $\tan\beta$ [67]. For large pseudoscalar masses or small values of $\tan\beta$, the supersymmetric contributions are suppressed, and the branching fraction approaches the Standard Model prediction.

# Chapter 6

# Summary of Results

In Paper 1 and Paper 2, we study stop squark as a next-to-lightest supersymmetric particle (NLSP) in the constrained MSSM. The stop NLSP scenario is phenomenologically motivated. In the cMSSM, the neutralino LSP is typically bino-like, which in large parts of the parameter space results in an excessive dark matter density because the annihilation cross section to fermions is suppressed. However, coannihilations between the lightest neutralino and the NLSP can bring the relic density down by enhancing the dilution of supersymmetric particles. This requires that the NLSP mass is close to the mass of the lightest neutralino. When stop is nearly degenerate with the LSP, a bino-like neutralino can explain the observed dark matter density. There is also an interesting connection between a light stop mass and the Higgs boson in the cMSSM. To obtain the $\sim$125 GeV mass for the Higgs boson without large stop masses, the stop mixing terms that appear in the one-loop correction for the Higgs mass are required provide a nearly maximal contribution. This maximal mixing scenario implies significant stop mixing and a light stop.

The effects of the renormalization group equations in the cMSSM are important in determining the NLSP since the RGEs are used to determine the low energy scale values of the soft supersymmetry breaking terms from the high energy scale input parameters of the model. Stop can be the NLSP when the off-diagonal mixing term $M_{LR}^2 = m_t(A_t - \mu \cot \beta)$ of the left- and right-handed top squark fields is large. A large $A_t$ parameter can cause one of the stop soft mass parameters to be driven to a small value, and a large mixing term reduces the mass of the lighter stop mass eigenstate $\tilde{t}_1$. In the squark and slepton soft mass term RGEs, the squared soft trilinear terms and the terms proportional to the Yukawa couplings (and scalar masses) decrease the soft mass parameters, while the terms proportional to the gauge couplings (and gaugino masses) have an opposite effect. The large top Yukawa coupling suggests that stop is lighter than the other squarks, but because the coupling constant of strong interactions is large, the stop mass parameters tend to increase faster than the slepton mass parameters as the gaugino mass scale increases. Therefore, a small gaugino mass parameter $m_{1/2}$ as compared to the scalar mass parameter

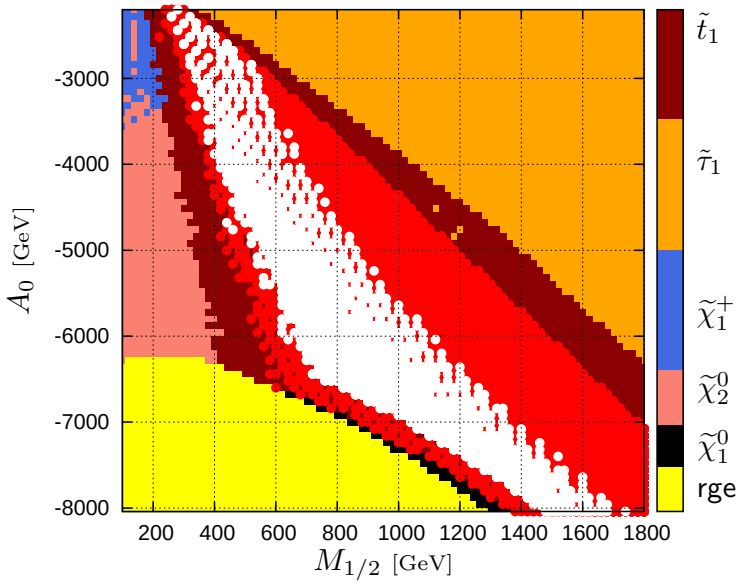


Figure 6.1: The potential stop NLSP area in the $m_{1/2} - A_0$ plane. The red points are the stop NLSP points with relic density below the WMAP upper limit, and the white subset of the points also obey the other constraints. The yellow area denoted by rge shows the parameter space where a viable solution for the particle spectrum does not exist. From Paper 1.

$m_0$ is favored.

To find the parameter points where stop is the NLSP and the experimental constraints are satisfied, we scanned the 4-dimensional parameter space of the cMSSM ($m_0, m_{1/2}, A_0$, and $\tan\beta$) with the sign of $\mu$ chosen to be positive and calculated the low energy particle spectrum and the constraints for each point with the SOFTSUSY [68] and micrOMEGAs [69] software packages. For the Higgs mass constraint, we used the LEP2 mass limit $m_h > 114$ GeV, which at the time was the experimental mass limit. The other constraints we used are the WMAP relic density bounds, the branching fractions of $b \to s\gamma$, $B \to \tau\nu$, and $B_s \to \mu^+\mu^-$. The results of the parameter scan for the interesting negative values of $A_0$ are presented in Fig. 6.1 as a projection in the $m_{1/2} - A_0$ plane.

In the scan, the scalar mass parameter is varied in the range 1000 GeV $\leq m_0 \leq$ 2848 GeV in steps of 66 GeV, and the ratio of the Higgs vevs is varied in the range $2.5 \leq \tan\beta \leq 55$ in steps of 0.5 up to the value 20, and in steps of 5 starting from the value 25. For the plot, we have weakened the relic density bound to include only the upper limit. In the red points, it is possible to choose $m_0$ and $\tan\beta$ in such a way that stop is the NLSP and the relic density is below the WMAP upper limit. The white points are a subset of these points where the rest of the constraints are not violated. The areas labeled by the sparticles names indicate the possible identity of the NLSP in the order of

preference starting from stop and continuing to the sparticles listed below it. For example, in the $\tilde{\tau}_1$ denoted points at least one stau NLSP point (but not a single stop NLSP point) was found by varying the $m_0$ and $\tan\beta$ parameters. The black area corresponds to parameter points where the lightest neutralino is not the LSP.

We find that there is a large area of potential stop NLSP points in the cMSSM for both positive and negative values of $A_0$. With a positive sign for $\mu$, the stop mixing term is larger for the negative $A_0$. The potential stop NLSP area is therefore larger for the negative trilinear soft term with our choice of positive $\mu$. If $|A_0|$ is much larger than $m_0$, there is a possibility that a color- and charge-breaking (CCB) minimum forms in the scalar potential that is deeper than the electroweak minimum [70]. However, quantum tunneling from the false vacuum, where only the neutral Higgs fields have vevs, to the true minimum may take a very long time [71]. For this reason, the existence of a CCB minimum does not automatically exclude the point in the parameter space. For all of the points we checked, the lifetime of the electroweak vacuum is longer than the age of the universe even if a CCB minimum develops. In the plot, the constraint that separates the white points from the red points is in most cases the Higgs mass limit. The Higgs maximal mixing area coincides well with the white subset, which implies that in many of these points the Higgs mass could easily be larger than the LEP2 bound we use.

In the area of potential stop NLSP points where the decay constraints and the Higgs mass limit are satisfied, it is possible to find points where the relic density agrees with the WMAP observations. These good points are a subset of the white points in Fig. 6.1. A typical mass spectrum of the points that can explain dark matter and satisfy our other constraints is shown in Fig. 6.2 as a function of stop mass. Stop is nearly degenerate with the lightest neutralino because efficient coannihilations require a small mass difference between the bino-like neutralino LSP and the stop NLSP. The relation between the mass difference and the relic density in our allowed stop NLSP points is plotted in Fig. 6.3. For stop masses smaller than 800 GeV, the mass difference is less than ∼50 GeV. This heavily restricts the possible decay modes of stop. The rest of the colored scalars are much heavier than the NLSP, and the lightest charginos and the second lightest neutralino are relatively light compared with squarks and sleptons. There is a clear correlation between the gluino and stop masses because the gaugino masses are related at the observable energy scale. The RGE evolution predicts that there is a mass relation $M_3 : M_1 \sim 6$, which corresponds to the ratio of gluino and bino-like neutralino masses, and the relic density constraint demands that stop is only slightly heavier than the LSP.

At the LHC, the direct stop production for a typical particle spectrum in our stop NLSP scenario is dominant over the stop production mechanisms that arise from cascade decays of other sparticles. This is because the direct production cross sections of gluinos and other squarks, which are much heavier than stop, are a lot smaller in comparison. When stop is the NLSP and $m_{\tilde{t}_1} - m_{\tilde{\chi}_1^0} < m_W$, the only kinematically possible stop decay channels are $\tilde{t}_1 \to u\tilde{\chi}_1^0$, $\tilde{t}_1 \to c\tilde{\chi}_1^0$, and $\tilde{t}_1 \to bf\bar{f}'\tilde{\chi}_1^0$. The first two of these are loop-induced

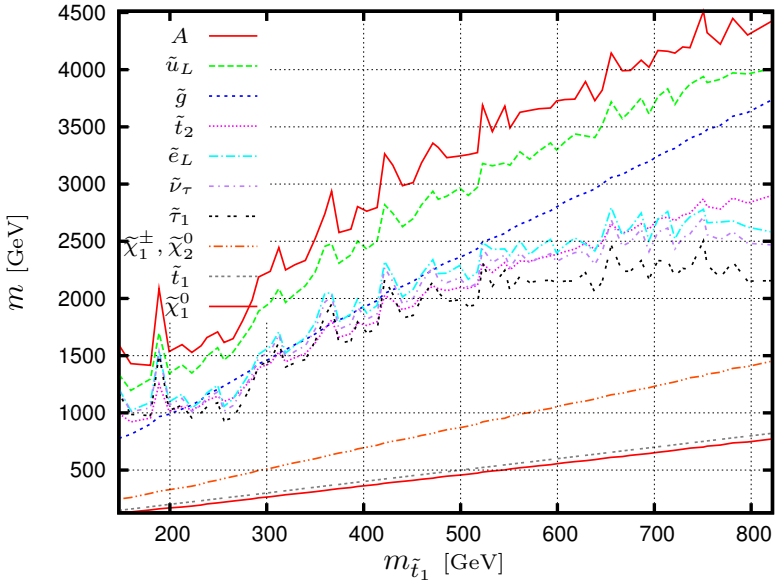


Figure 6.2: Mass spectrum of a set of good stop NLSP points as a function of the stop mass. In the key, particles are listed in descending mass order found at $m_{\tilde{t}_1} = 800$ GeV. Relic density satisfies the WMAP constraint. From Paper 1.

decays, whereas the four-body decays occur at tree-level. The decay channel $\tilde{t}_1 \to c\tilde{\chi}_1^0$ is likely dominant over the four-body decay since it receives a large logarithmic enhancement from renormalization group evolution [72]. Although the other loop decay is similarly enhanced, it is suppressed by a small quark mixing matrix element. In Fig. 6.4, we have plotted the branching fractions of the largest decay channels, which we computed with SUSY-HIT [73], as a function of stop mass for the points in Fig. 6.2. The four-body decay becomes more important as the mass difference between stop and neutralino grows. We conclude Paper 1 with discussion about the possible collider signals of the stop NLSP scenario at the LHC. The production of stops and associated particles from decays of heavy gluinos suffer from small production cross sections, while direct production of stops followed by the dominant decay to charm quarks and neutralinos leads to a challenging signature consisting of two jets and missing energy. The small mass difference of the two lightest supersymmetric particles results in that the $c$ jets are soft, so the signal of the light stops can easily be lost in the background because soft jets are also produced in abundance in ordinary QCD processes.

In Paper 2, we propose an interesting signature of the stop NLSP scenario in the cMSSM. Signatures of light stops with a dominant decay channel to a charm quark and the lightest neutralino have been studied, for example, in the case of direct stop production in association with $b$ jets [74], single photon [75],

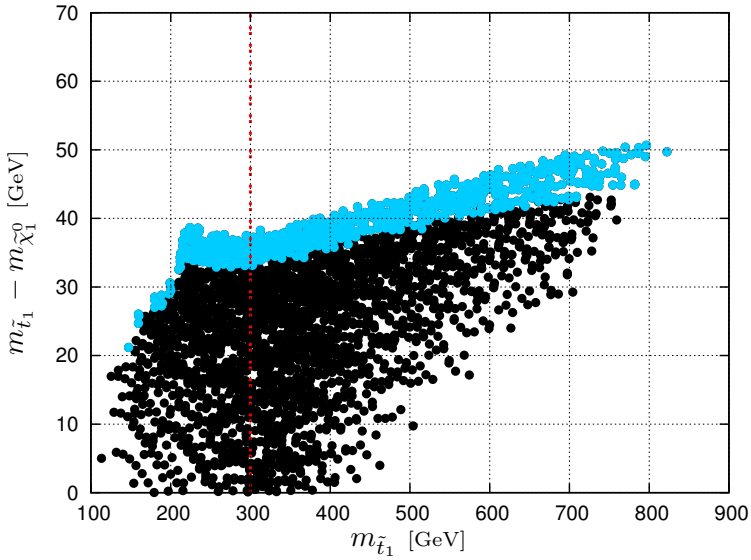


Figure 6.3: Mass difference of the two lightest supersymmetric particles. For the black dots the relic density is smaller than the WMAP upper bound, and for the light blue dots the relic density is within the WMAP limits. From Paper 1.

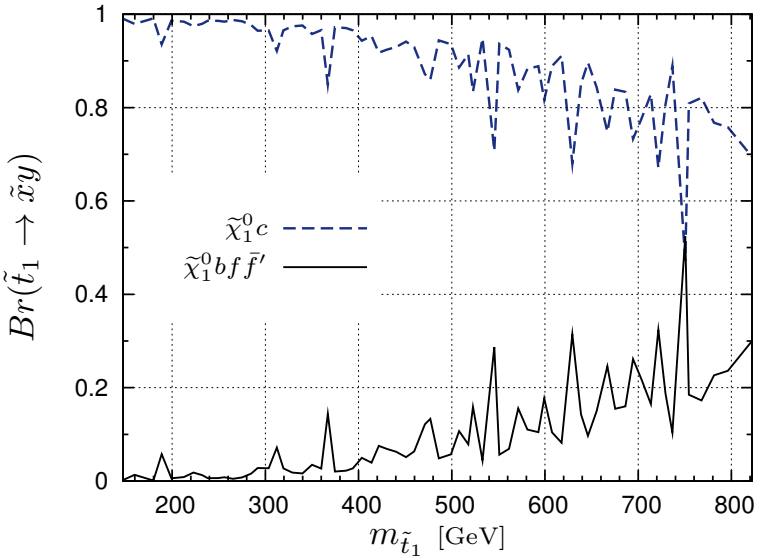


Figure 6.4: Branching fractions of the two most important stop decay channels. From Paper 1.

or a single jet [76], and in the case of stop production from gluino decays leading to a pair of same-sign top quarks and stops [77]. The ATLAS experiment has searched for stops in the decay channel $\tilde{t}_1 \rightarrow c\tilde{\chi}_1^0$ at center of mass energy $\sqrt{s} = 8$ TeV with 20.3 inverse femtobarns of collision data [78]. The ATLAS results exclude stop masses up to about 250 GeV.

The signature we present is based on gluino-mediated production of stops. Gluinos will decay dominantly to a stop and a top quark, $\tilde{g} \rightarrow \bar{t}\tilde{t}_1$ or $\tilde{g} \rightarrow t\tilde{t}_1^*$, and stops will subsequently decay in the dominant channel $\tilde{t}_1 \rightarrow c\tilde{\chi}_1^0$, so the pair production of gluinos results in two top quarks, two charm quarks, and two lightest neutralinos. Even though the gluino production cross section is small in comparison with the stop production cross section due to gluinos being $\sim$5 times more massive than stops in the model, the mass difference in combination with the two top quarks as decay products gives rise to a signature that allows to reject the background without sapping the signal strength. Since gluino is much heavier than stop, stops and top quarks from the gluino decays will be boosted. The lightest neutralino from the stop decay carries most of the boosted stop's momentum, while the $c$ jet from the hadronization of the light charm quark is soft. Top quarks decay dominantly to a bottom quark and a $W$ boson. One way to identify the decay is by finding the resulting $b$ jet. But in this case $b$-tagging is difficult, since the boosted top quarks decay to produce sets of collimated particles that appear as single jets. Another issue is that when the top decays are searched in the dominant hadronic decay channel of the $W$ boson, the signal is susceptible to a large background. The background can be reduced by selecting only events where at least one of the $W$ boson decays results in an isolated lepton. However, the branching fraction for the semileptonic top decay is smaller than for the hadronic decay, and a highly boosted top often leads to a non-isolated lepton [79]. To find boosted tops, instead of searching for bottom quarks and isolated leptons, it is more efficient to use top tagging algorithms that identify the hadronically decaying boosted top quarks by analyzing the substructure of the jets and the energy distribution in the events. In the analysis of the signature, we use the Johns Hopkins top tagger algorithm [80].

We study two high transverse momentum top jets plus large missing energy as a signature of the stop NLSP scenario in the cMSSM. The gluino-gluino, squark-gluino and squark-squark production cross sections at the LHC with $\sqrt{s} = 14$ TeV were calculated with Prospino 2.1 [81], and the event generation was done with Pythia 6.4, whereas FastJet 3 [82] handled the jet analysis. The largest Standard Model backgrounds for the signature arise from $t\bar{t}$ and QCD multijet production. In addition, $t\bar{t}$ production processes associated with a vector boson, $t\bar{t}Z$ and $t\bar{t}W$, can contribute to the background. All of these SM backgrounds also give rise to missing energy because of detector resolution effects, which we have simulated by smearing the jet energies. The $t\bar{t}$ and multijet backgrounds were simulated with Pythia, while the $t\bar{t}$ with a vector boson processes were simulated with ALPGEN [83] and Pythia. In the analysis of the signal, we select events that contain at least two top tagged jets with $p_T \geq 500$ GeV and pseudorapidity $|\eta| \leq 2.5$, and reject events with one or

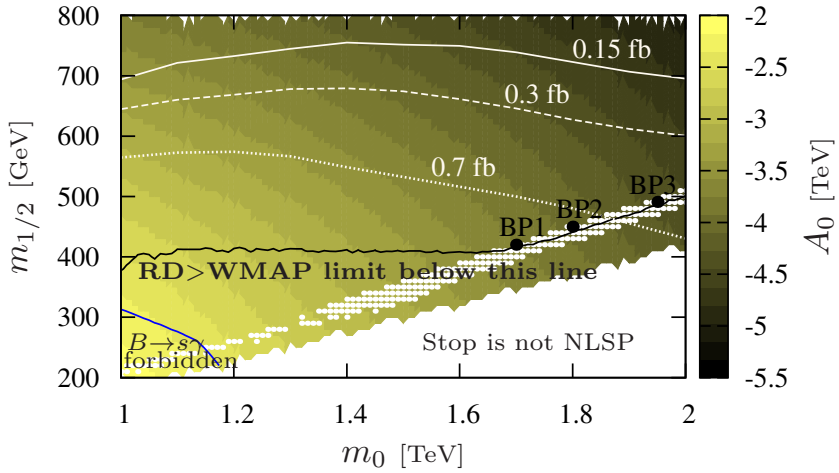


Figure 6.5: The three-dimensional parameter space that gives rise to a stop NLSP for $\tan\beta = 15$ and $\mu > 0$. To select a particular value for $A_0$ we demand $m_{\tilde{t}_1} - m_{\tilde{\chi}_1^0} \sim 35$ GeV when possible. The white dots correspond to the points resulting in a $m_h \sim 125 \pm 2$ GeV. Constant signal cross-section contours in the $m_0 - m_{1/2}$ plane after acceptance cuts + $\not{E}_T \geq 500$ GeV at the 14 TeV LHC are also shown in the plot. From Paper 2.

more isolated electrons or muons with $p_T \geq 20$ GeV and $|\eta| \leq 2.5$. These are our event acceptance cuts. We find that the acceptance cuts together with a large missing energy requirement efficiently reject the background without destroying the signal cross section. The predicted number of background events for $\not{E}_T \geq 500$ GeV with 100 inverse femtobarns of integrated luminosity is less than one.

In Fig. 6.5, stop NLSP points are plotted for $\tan\beta = 15$ and $\mu > 0$. For each point, the particle spectrum was calculated with SuSpect [84], and the constraints were checked with micrOMEGAs [69]. In the three benchmark points, the relic density agrees with the WMAP limits and the experimental decay constraints are fulfilled. The gluino and stop masses in the BP3 are $m_{\tilde{g}} = 1227$ GeV and $m_{\tilde{t}_1} = 250$ GeV. With a missing energy cut $\not{E}_T \geq 500$ GeV, the signal cross section for BP3 is 0.57 fb. If we require 5(10) signal events for discovery, this point will be probed at the 14 TeV LHC with 9(18) fb$^{-1}$ of collision data. Constant signal cross section contours are displayed for 0.7, 0.3, and 0.15 fb in the $m_0 - m_{1/2}$ plane corresponding to gluino masses $m_{\tilde{g}}$~1.1, 1.5, and 1.7 TeV at high $m_0$. These will be probed with 7(13), 17(33), and 33(67) fb$^{-1}$ of data for 5(10) signal events.

The two high $p_T$ top jets and missing energy signature can be used to extract the signal of the stop NLSP scenario even when stop is not nearly degenerate with the lightest neutralino. In Fig. 6.6, the signal cross sections for the acceptance cuts with $\not{E}_T \geq 500$ GeV are plotted as a function of stop mass. To obtain different stop masses, we have varied the $A_0$ parameter while

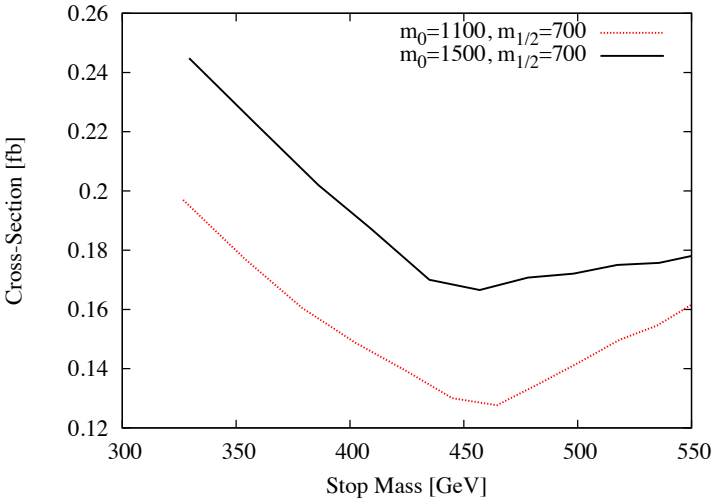


Figure 6.6: Signal cross sections as a function of stop mass for two different sets of $m_0 - m_{1/2}$ after acceptance cuts + $\not{E}_T \geq 500$ GeV at the 14 TeV LHC, $\tan\beta = 15$ and $\mu > 0$ are assumed. From Paper 2.

keeping $m_0$ and $m_{1/2}$ fixed. Initially, the signal cross section decreases as the stop mass increases, because a smaller mass splitting between the gluino and stop means less boosted top quarks. For $m_{1/2} = 700$ GeV, the lightest neutralino mass is ∼300 GeV. When the stop mass is above ∼475 GeV, an additional decay channel $\tilde{t}_1 \to t\tilde{\chi}_1^0$ opens up. This increases the possibility of obtaining more boosted top jets, which results in a larger signal cross section. The signal cross section stays fairly constant as long as stop is the NLSP, so the signature is applicable to the whole parameter space where stop is the NLSP in the cMSSM. The signature allows to probe stops with masses up to 550 GeV in the presence of a gluino with mass below 1.7 TeV at the 14 TeV LHC with 33 fb$^{-1}$ of integrated luminosity.

In Paper 3, we investigate right-handed sneutrino and neutralino dark matter in the NMSSM with a right-handed neutrino and spontaneous violation of CP symmetry. The cosmological baryon asymmetry suggests that an additional source of CP violation beyond what the Standard Model provides is needed. The soft supersymmetry breaking terms can have complex phases and consequently introduce CP violating effects, but the phases are severely constrained by experiments such as the measurement of the electric dipole moment (EDM) of the electron. Another way to introduce CP violation is by demanding that the Lagrangian is CP conserving and then breaking the symmetry spontaneously by complex expectation values of the Higgs fields. In this case, there are far fewer CP-violating parameters in the model. In the MSSM, however, spontaneous violation of CP is not possible at tree-level because the minimum of the scalar potential is real. This leads us to consider

extended supersymmetric models. The lightest right-handed sneutrino in the NMSSM is an interesting candidate for dark matter. The singlet Higgs superfield in the model allows right-handed sneutrinos to have electroweak scale interactions. This means right-handed sneutrinos can be thermally produced in the early universe, and since they have a reduced coupling to the $Z$ boson, they can produce the correct relic density. In contrast, left-handed sneutrinos self-annihilate too efficiently to explain dark matter. Right-handed sneutrino dark matter in the NMSSM has been studied in [85, 86], and neutralino dark matter in the NMSSM in, for example, [87, 88].

For the numerical analysis, we implemented the model with LanHEP [89] and analyzed it with micrOMEGAs [69]. The EDM constraint was checked with a dedicated Mathematica code. To satisfy the EDM constraint, the CP-violating Higgs vev phases are generally restricted to small values. The B-physics constraints BR($B \to X_s\gamma$), BR($B^+ \to \tau^+\nu_\tau$), and BR($B_s \to \mu^+\mu^-$) were calculated using NMSSMtools [90]. Even though the NMSSMtools model does not feature CP violation or right-handed neutrinos, we argue that they do not have much of an effect on the results of the calculation in the case of small phases. Other constraints we use include the PDG limits [91] on the sparticle masses, and the coupling strengths of the Higgs bosons to the $Z$ bosons. We also require that a Standard Model-like Higgs boson with a mass between 123-128 GeV is in the spectrum. For our analysis of the effects of the CP-violating phases, we generated two data sets: one with CP-conserving phases, and one where the phases were randomly varied and limited to small values (modulo $\pi$). In both sets the parameters that affect the Higgs and sneutrino spectra as well as the interactions of the dark matter candidate were randomly varied. The gaugino masses were kept fixed to see the effect of the bino dominance in the neutralino LSP, and the squark mass parameters were chosen in such a way that the squark masses were above the experimental limits.

If the CP-violating phases are small, a light Higgs boson $h_S$ appears in the spectrum [92]. This Higgs state is singlet dominated, so it can be much lighter than the observed Standard Model-like Higgs boson while still being consistent with experimental constraints because of its reduced coupling to the $Z$ bosons. The change in the Higgs spectrum occurs discontinuously when CP is spontaneously violated by small phases. The small phases also cause the masses of the supersymmetric particles to change, but since this change occurs continuously, the mass spectrum is very close to the CP-conserving spectrum. We find that the light singlet dominated Higgs has very little effect on the B-physics constraints because it first appears in the calculations of the branching fractions at two-loop order. In the case of relic density, a light $h_S$ can open new annihilation channels depending on the type and composition of the LSP and thus increase the annihilation rate of dark matter.

The lightest neutralino can have a significant singlino admixture. The annihilation channels unsuppressed by the singlino component into a pair of fermions are available only if the right-handed neutrino $\nu_R$ is lighter than the LSP. However, both the annihilation cross sections and $m_{\nu_R}$ depend on the $\lambda_N$ coupling, so a small $m_{\nu_R}$ can lead to a suppression of the annihilation rate

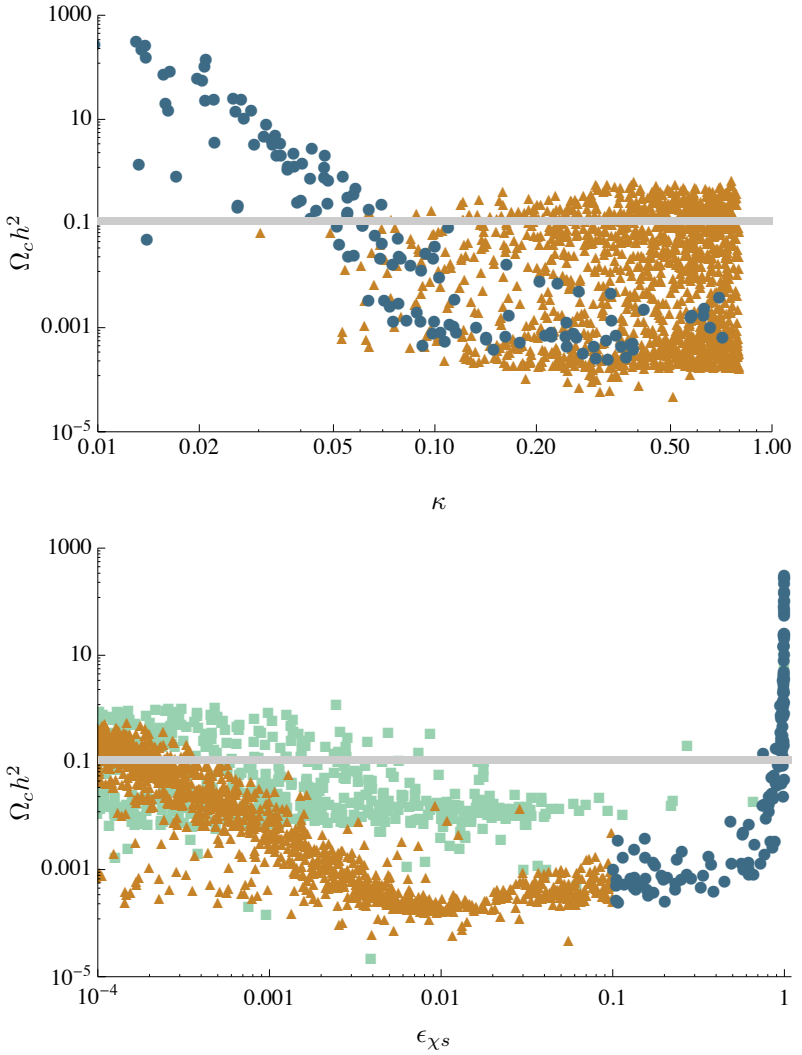


Figure 6.7: Top: The relic density against the trilinear coupling $\kappa$ for neutralino LSPs. Bottom: The relic density against the singlino component of the neutralino LSP. Points with (blue circles) and without (orange triangles) significant singlino component. Green boxes depict points from the CP-conserving data set. The grey band indicates the current WMAP limits on the relic density. From Paper 3.

in this channel. If $h_S$ is light, the most important annihilation channels in reducing the relic density of a singlino-like LSP are the ones with a $h_S h_S$ final state. These channels are dependent on the square of the trilinear coupling $\kappa$. We denote the singlino component of the neutralino LSP as $\epsilon_{\chi s}$, and in Fig. 6.7 we show the effect of $\kappa$ and $\epsilon_{\chi s}$ on the relic density. For neutralino LSPs with a considerable singlino component (blue circles), the small values of $\kappa \lesssim 0.05$ correspond to large relic density. This is because the neutralino mixing is controlled by the $\kappa$ parameter, and the small values of $\kappa$ result in the LSP being highly singlino dominated. The relic density increases as $\kappa$ gets smaller, since the annihilation channels into $h_S h_S$ become less effective. We see the effect of the light $h_S$ on the relic density of neutralinos in the bottom plot. A growing singlino component decreases the relic density when the light $h_S$ final state annihilation channels are available. As a result, the relic density is generally lower than in the CP-conserving case, which is depicted by the green boxes, beginning from $\epsilon_{\chi s} \gtrsim 0.001$. For highly singlino dominated neutralinos, the annihilation channels are again suppressed by small $\kappa^2$.

We find that the relic density of right-handed sneutrinos in the CP-violating case is generally lower than in the CP-conserving case. This is also a result of the new final state $h_S$ in the annihilations. These annihilation channels are sensitive to $\lambda_N$. In Fig. 6.8, we plot the relic density of neutralino and sneutrino dark matter. In the top plot, the fixed gaugino mass parameter $M_1 = 300$ GeV leads to a bino-like neutralino and large relic density at $m_{\chi_1^0} = M_1$. At lower masses, the doublet dominated LSP is more higgsino-like, which decreases the relic density. For the doublet dominated lightest neutralinos, the relic density is generally smaller in the CP-violating case than in the CP-conserving case, as previously noted. Only the singlino dominated LSPs can saturate the relic density limits at lower masses. In the bottom plot, we see that the right-handed sneutrino is able to produce the observed relic density, whereas the left-handed sneutrino is a poor dark matter candidate. There are only a few points in both of the plots where all the experimental constraints are satisfied. We find that the electron EDM is the most restrictive constraint.

Fig. 6.9 shows the LSP mass versus the spin independent cross section for a set of CP-violating points and the XENON100 and LUX dark matter direct detection limits. The LUX direct detection limit is a strong constraint since it rules out a large portion of the parameter points. Most of the right-handed sneutrino points allowed by the direct detection limit are forbidden by the WMAP constraint, but some viable points still remain. A large number of neutralino LSP points are allowed by both constraints.

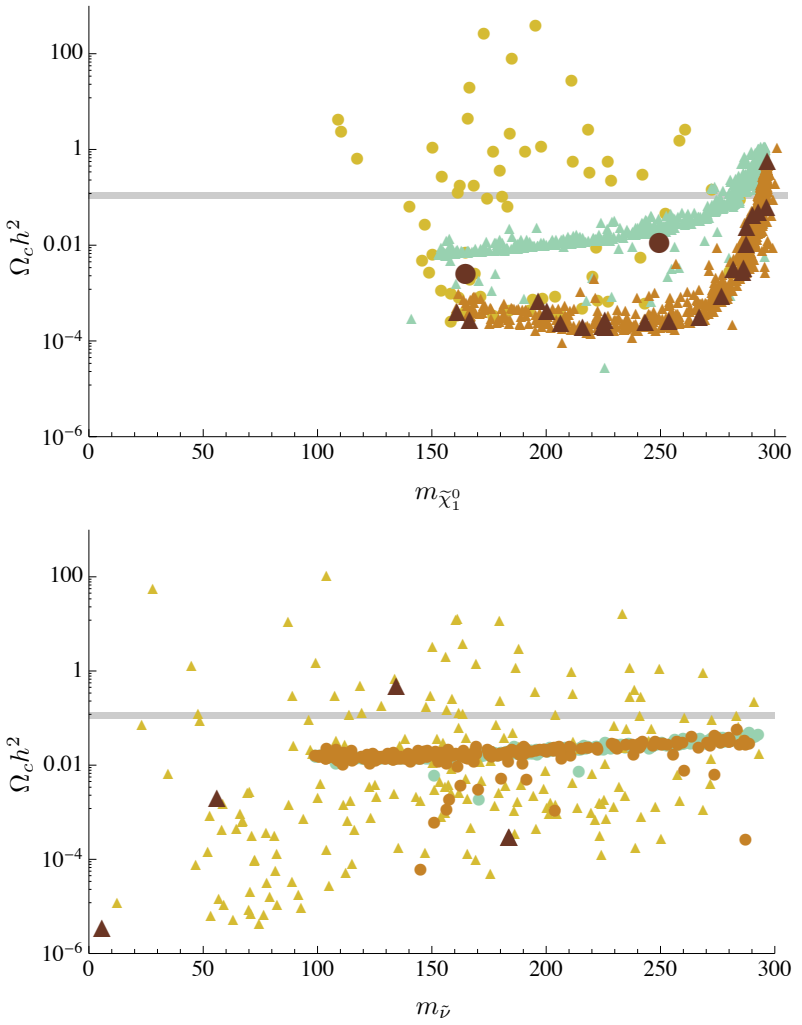


Figure 6.8: The relic density against the LSP mass. Top: for neutralino LSPs in the CP-conserving (light green triangle), CP-violating doublet dominated (orange triangle) and CP-violating significant singlino admixture, i.e. $\epsilon_{\chi s} > 0.1$, (yellow dot) cases. Bottom: for sneutrino LSPs in the CP-violating left-handed (orange dot) and CP-violating right-handed (yellow triangle) case. The CP-conserving left-handed (light green dot) set overlaps completely with the CP-violating counterpart. In both plots all points satisfy PDG constraints on the mass spectrum and vacuum stability, large brown triangles or circles indicate points that pass all of the other experimental constraints we impose. The grey band indicates the current WMAP limits on the relic density. From Paper 3.

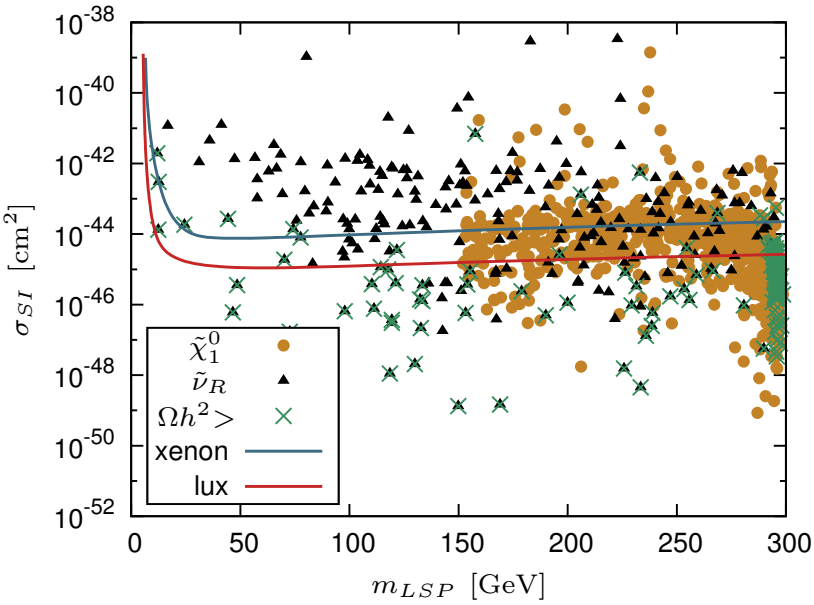


Figure 6.9: Spin-independent WIMP–nucleon cross section for CPV points. Points with triangular shape (black) have the right-handed sneutrino as an LSP, while the dots (orange) have neutralino LSP. The (green) cross above a point corresponds to a relic density above the WMAP upper limit, hence an excluded point. The solid lines represent the XENON100 and LUX experimental limits. From Paper 3, with the LUX results additionally plotted.

# Chapter 7

# Conclusions

Supersymmetry is a promising theory for new physics at the TeV scale. The main motivation for supersymmetry is that it can stabilize the electroweak scale and therefore provide a solution to the hierarchy problem. Supersymmetric models have also other compelling features such as gauge coupling unification, and the fact that they can offer viable dark matter candidates if R-parity is conserved.

Searches of supersymmetric particles at the LHC have so far come up empty. The implication is that gluinos and first and second generation squarks are expected to have masses above one TeV, while neutralinos, charginos, sleptons, and third generation squarks are still allowed to be significantly lighter. A light stop is particularly interesting when it is the next-to-lightest supersymmetric particle in the cMSSM. In this scenario, which is explored in Paper 1, stop coannihilations can dilute the relic density to such an extent that the lightest neutralino can explain dark matter. The stop NLSP scenario leads to an interesting signature consisting of large missing energy and boosted top jets from gluino decays at the LHC, as shown in Paper 2. This allows to significantly reduce the Standard Model background.

One of the attractive features of extended supersymmetric models with a singlet Higgs superfield is that they can solve the $\mu$ problem. The MSSM can also be extended further to include right-handed neutrino superfields, which can give rise to the neutrino masses. Moreover, a right-handed sneutrino as a thermal relic can provide the observed dark matter density. When spontaneous CP violation is introduced in the NMSSM with a right-handed neutrino by small complex phases, a light singlet scalar appears in the spectrum, which provides new annihilation channels for neutralinos and right-handed sneutrinos. Neutralino and sneutrino dark matter in this model is investigated in Paper 3.

The LHC will begin its second run in 2015 with an increased collision energy. By the end of the run, squarks and gluinos with multi-TeV masses are expected to be within reach, so if supersymmetry has a role in TeV scale physics, the experiments should have a good chance of finding supersymmetric particles.

If supersymmetric particles are discovered, the measurement of their properties could illuminate deeper structures such as the pattern of supersymmetry breaking and the origin of the suppression of flavor changing and CP-violating effects, and thus reveal aspects of more fundamental physics at energy scales far beyond what can be directly probed.

# Bibliography


[1] S. P. Martin, *A Supersymmetry primer*, *Adv.Ser.Direct.High Energy Phys.* **21** (2010) 1–153, [hep-ph/9709356].

[2] S. R. Coleman and J. Mandula, *All Possible Symmetries of the S Matrix*, *Phys.Rev.* **159** (1967) 1251–1256.

[3] R. Haag, J. T. Lopuszanski, and M. Sohnius, *All Possible Generators of Supersymmetries of the S-Matrix*, *Nucl.Phys.* **B88** (1975) 257.

[4] M. Sohnius, *Introducing Supersymmetry*, *Phys.Rept.* **128** (1985) 39–204.

[5] I. J. Aitchison, *Supersymmetry and the MSSM: An Elementary introduction*, hep-ph/0505105.

[6] L. Girardello and M. T. Grisaru, *Soft Breaking of Supersymmetry*, *Nucl.Phys.* **B194** (1982) 65.

[7] H. Baer and X. Tata, *Weak Scale Supersymmetry: From Superfields to Scattering Events*. Cambridge University Press, 2006.

[8] F. Gabbiani, E. Gabrielli, A. Masiero, and L. Silvestrini, *A Complete analysis of FCNC and CP constraints in general SUSY extensions of the standard model*, *Nucl.Phys.* **B477** (1996) 321–352, [hep-ph/9604387].

[9] Y. Grossman, Y. Nir, and R. Rattazzi, *CP violation beyond the standard model*, *Adv.Ser.Direct.High Energy Phys.* **15** (1998) 755–794, [hep-ph/9701231].

[10] A. G. Cohen, D. Kaplan, and A. Nelson, *The More minimal supersymmetric standard model*, *Phys.Lett.* **B388** (1996) 588–598, [hep-ph/9607394].

[11] F. Brummer, S. Kraml, and S. Kulkarni, *Anatomy of maximal stop mixing in the MSSM*, *JHEP* **1208** (2012) 089, [arXiv:1204.5977].

[12] G. Giudice and A. Masiero, *A Natural Solution to the mu Problem in Supergravity Theories*, *Phys.Lett.* **B206** (1988) 480–484.

[13] U. Ellwanger, C. Hugonie, and A. M. Teixeira, *The Next-to-Minimal Supersymmetric Standard Model*, *Phys.Rept.* **496** (2010) 1–77, [arXiv:0910.1785].

[14] S. Abel, S. Sarkar, and P. White, *On the cosmological domain wall problem for the minimally extended supersymmetric standard model*, *Nucl.Phys.* **B454** (1995) 663–684, [hep-ph/9506359].

[15] C. Panagiotakopoulos and K. Tamvakis, *Stabilized NMSSM without domain walls*, *Phys.Lett.* **B446** (1999) 224–227, [hep-ph/9809475].

[16] Intensity Frontier Neutrino Working Group, A. de Gouvea *et. al.*, *Working Group Report: Neutrinos*, arXiv:1310.4340.

[17] Planck Collaboration, P. Ade *et. al.*, *Planck 2013 results. I. Overview of products and scientific results*, *Astron.Astrophys.* **571** (2014) A1, [arXiv:1303.5062].

[18] R. Mohapatra, *Theories of neutrino masses and mixings*, hep-ph/9910365.

[19] G. Jungman, M. Kamionkowski, and K. Griest, *Supersymmetric dark matter*, *Phys.Rept.* **267** (1996) 195–373, [hep-ph/9506380].

[20] G. Bertone, D. Hooper, and J. Silk, *Particle dark matter: Evidence, candidates and constraints*, *Phys.Rept.* **405** (2005) 279–390, [hep-ph/0404175].

[21] D. Clowe, M. Bradac, A. H. Gonzalez, M. Markevitch, S. W. Randall, *et. al.*, *A direct empirical proof of the existence of dark matter*, *Astrophys.J.* **648** (2006) L109–L113, [astro-ph/0608407].

[22] C. J. Copi, D. N. Schramm, and M. S. Turner, *Big bang nucleosynthesis and the baryon density of the universe*, *Science* **267** (1995) 192–199, [astro-ph/9407006].

[23] S. Burles, K. M. Nollett, and M. S. Turner, *Big bang nucleosynthesis predictions for precision cosmology*, *Astrophys.J.* **552** (2001) L1–L6, [astro-ph/0010171].

[24] Planck Collaboration, P. Ade *et. al.*, *Planck 2013 results. XVI. Cosmological parameters*, *Astron.Astrophys.* **571** (2014) A16, [arXiv:1303.5076].

[25] WMAP, C. Bennett *et. al.*, *Nine-Year Wilkinson Microwave Anisotropy Probe (WMAP) Observations: Final Maps and Results*, *Astrophys.J.Suppl.* **208** (2013) 20, [arXiv:1212.5225].

[26] A. Kusenko, *Sterile neutrinos: The Dark side of the light fermions*, *Phys.Rept.* **481** (2009) 1–28, [arXiv:0906.2968].

[27] K. Griest and D. Seckel, *Three exceptions in the calculation of relic abundances*, *Phys.Rev.* **D43** (1991) 3191–3203.

[28] H. Baer, V. Barger, and A. Mustafayev, *Neutralino dark matter in mSUGRA/CMSSM with a 125 GeV light Higgs scalar*, *JHEP* **1205** (2012) 091, [arXiv:1202.4038].

[29] K.A. Olive et al. (Particle Data Group), *2014 Review of Particle Physics*, *Chin. Phys. C* **38** (2014) 090001.

[30] R. Bernabei, P. Belli, F. Cappella, V. Caracciolo, S. Castellano, *et. al.*, *Final model independent result of DAMA/LIBRA-phase1*, *Eur.Phys.J.* **C73** (2013) 2648, [arXiv:1308.5109].

[31] G. Angloher, M. Bauer, I. Bavykina, A. Bento, C. Bucci, *et. al.*, *Results from 730 kg days of the CRESST-II Dark Matter Search*, *Eur.Phys.J.* **C72** (2012) 1971, [arXiv:1109.0702].

[32] CDMS Collaboration, R. Agnese *et. al.*, *Silicon Detector Dark Matter Results from the Final Exposure of CDMS II*, *Phys.Rev.Lett.* **111** (2013) 251301, [arXiv:1304.4279].

[33] CoGeNT collaboration, C. Aalseth *et. al.*, *Results from a Search for Light-Mass Dark Matter with a P-type Point Contact Germanium Detector*, *Phys.Rev.Lett.* **106** (2011) 131301, [arXiv:1002.4703].

[34] CoGeNT Collaboration, C. Aalseth *et. al.*, *Search for An Annual Modulation in Three Years of CoGeNT Dark Matter Detector Data*, arXiv:1401.3295.

[35] CDMS Collaboration, Z. Ahmed *et. al.*, *Search for annual modulation in low-energy CDMS-II data*, arXiv:1203.1309.

[36] XENON100 Collaboration, E. Aprile *et. al.*, *Dark Matter Results from 225 Live Days of XENON100 Data*, *Phys.Rev.Lett.* **109** (2012) 181301, [arXiv:1207.5988].

[37] LUX Collaboration, D. Akerib *et. al.*, *First results from the LUX dark matter experiment at the Sanford Underground Research Facility*, *Phys.Rev.Lett.* **112** (2014) 091303, [arXiv:1310.8214].

[38] C. Weniger, *A Tentative Gamma-Ray Line from Dark Matter Annihilation at the Fermi Large Area Telescope*, *JCAP* **1208** (2012) 007, [arXiv:1204.2797].

[39] Fermi-LAT Collaboration, M. Ackermann *et. al.*, *Search for Gamma-ray Spectral Lines with the Fermi Large Area Telescope and Dark Matter Implications*, *Phys.Rev.* **D88** (2013) 082002, [arXiv:1305.5597].

[40] T. Daylan, D. P. Finkbeiner, D. Hooper, T. Linden, S. K. N. Portillo, *et. al.*, *The Characterization of the Gamma-Ray Signal from the Central Milky Way: A Compelling Case for Annihilating Dark Matter*, arXiv:1402.6703.

[41] PAMELA Collaboration, O. Adriani *et. al.*, *An anomalous positron abundance in cosmic rays with energies 1.5-100 GeV*, *Nature* **458** (2009) 607–609, [arXiv:0810.4995].

[42] Fermi LAT Collaboration, M. Ackermann *et. al.*, *Measurement of separate cosmic-ray electron and positron spectra with the Fermi Large Area Telescope*, *Phys.Rev.Lett.* **108** (2012) 011103, [arXiv:1109.0521].

[43] AMS Collaboration, M. Aguilar *et. al.*, *First Result from the Alpha Magnetic Spectrometer on the International Space Station: Precision Measurement of the Positron Fraction in Primary Cosmic Rays of 0.5–350 GeV*, *Phys.Rev.Lett.* **110** (2013) 141102.

[44] D. Hooper, P. Blasi, and P. D. Serpico, *Pulsars as the Sources of High Energy Cosmic Ray Positrons*, *JCAP* **0901** (2009) 025, [arXiv:0810.1527].

[45] ANTARES Collaboration, S. Adrian-Martinez *et. al.*, *First results on dark matter annihilation in the Sun using the ANTARES neutrino telescope*, *JCAP* **1311** (2013) 032, [arXiv:1302.6516].

[46] IceCube Collaboration, R. Abbasi *et. al.*, *Multi-year search for dark matter annihilations in the Sun with the AMANDA-II and IceCube detectors*, *Phys.Rev.* **D85** (2012) 042002, [arXiv:1112.1840].

[47] IceCube collaboration, M. Aartsen *et. al.*, *Search for dark matter annihilations in the Sun with the 79-string IceCube detector*, *Phys.Rev.Lett.* **110** (2013), no. 13 131302, [arXiv:1212.4097].

[48] Super-Kamiokande Collaboration, T. Tanaka *et. al.*, *An Indirect Search for WIMPs in the Sun using 3109.6 days of upward-going muons in Super-Kamiokande*, *Astrophys.J.* **742** (2011) 78, [arXiv:1108.3384].

[49] ATLAS Collaboration, G. Aad *et. al.*, *Observation of a new particle in the search for the Standard Model Higgs boson with the ATLAS detector at the LHC*, *Phys.Lett.* **B716** (2012) 1–29, [arXiv:1207.7214].

[50] CMS Collaboration, S. Chatrchyan *et. al.*, *Observation of a new boson at a mass of 125 GeV with the CMS experiment at the LHC*, *Phys.Lett.* **B716** (2012) 30–61, [arXiv:1207.7235].

[51] M. Kramer, A. Kulesza, R. van der Leeuw, M. Mangano, S. Padhi, *et. al.*, *Supersymmetry production cross sections in pp collisions at* $\sqrt{s} = 7$ *TeV*, arXiv:1206.2892.

[52] *Search for squarks and gluinos with the ATLAS detector in final states with jets and missing transverse momentum and 20.3 $fb^{-1}$ of $\sqrt{s} = 8$ TeV proton-proton collision data*, Tech. Rep. ATLAS-CONF-2013-047, CERN, Geneva, May, 2013.

[53] CMS, "CMS Supersymmetry Physics Results, https://twiki.cern.ch/twiki/bin/view/CMSPublic/PhysicsResultsSUS."

[54] ATLAS, "Summary plots from the ATLAS supersymmetry physics group, https://atlas.web.cern.ch/Atlas/GROUPS/PHYSICS/CombinedSummaryPlots/SUSY/."

[55] BaBar Collaboration, J. Lees *et. al.*, *Evidence of $B \to \tau\nu$ decays with hadronic $B$ tags*, *Phys.Rev.* **D88** (2013) 031102, [arXiv:1207.0698].

[56] Belle Collaboration, I. Adachi *et. al.*, *Measurement of $B^- \to \tau^- \bar{\nu}_\tau$ with a Hadronic Tagging Method Using the Full Data Sample of Belle*, *Phys.Rev.Lett.* **110** (2013) 131801, [arXiv:1208.4678].

[57] A. Akeroyd and S. Recksiegel *J.Phys.G* **G29** (2003) 2311–2317, [hep-ph/0306037].

[58] M. Misiak, H. Asatrian, K. Bieri, M. Czakon, A. Czarnecki, *et. al.* *Phys.Rev.Lett.* **98** (2007) 022002, [hep-ph/0609232].

[59] Heavy Flavor Averaging Group, Y. Amhis *et. al.*, *Averages of B-Hadron, C-Hadron, and tau-lepton properties as of early 2012*, arXiv:1207.1158.

[60] BaBar Collaboration, J. Lees *et. al.*, *Measurement of $B(B \to X_s\gamma)$, the $B \to X_s\gamma$ photon energy spectrum, and the direct CP asymmetry in $B \to X_{s+d}\gamma$ decays*, *Phys.Rev.* **D86** (2012) 112008, [arXiv:1207.5772].

[61] W. Altmannshofer, M. Carena, N. R. Shah, and F. Yu, *Indirect Probes of the MSSM after the Higgs Discovery*, *JHEP* **1301** (2013) 160, [arXiv:1211.1976].

[62] F. Domingo and U. Ellwanger, *Updated Constraints from B Physics on the MSSM and the NMSSM*, *JHEP* **0712** (2007) 090, [arXiv:0710.3714].

[63] A. J. Buras, R. Fleischer, J. Girrbach, and R. Knegjens, *Probing New Physics with the B_s to $\mu+$ $\mu-$ Time-Dependent Rate*, *JHEP* **1307** (2013) 77, [arXiv:1303.3820].

[64] CMS Collaboration, S. Chatrchyan *et. al.*, *Measurement of the B(s) to mu+ mu- branching fraction and search for B0 to mu+ mu- with the CMS Experiment*, *Phys.Rev.Lett.* **111** (2013) 101804, [arXiv:1307.5025].

[65] LHCb collaboration, R. Aaij *et. al.*, *Measurement of the $B_s^0 \to \mu^+\mu^-$ branching fraction and search for $B^0 \to \mu^+\mu^-$ decays at the LHCb experiment*, *Phys.Rev.Lett.* **111** (2013) 101805, [arXiv:1307.5024].

[66] CMS and L. Collaborations, *Combination of results on the rare decays $B^0_{(s)} \to \mu^+\mu^-$ from the CMS and LHCb experiments*, .

[67] A. Arbey, M. Battaglia, F. Mahmoudi, and D. Martinez Santos, *Supersymmetry confronts $B_s \to \mu^+\mu^-$: Present and future status*, *Phys.Rev.* **D87** (2013) 035026, [arXiv:1212.4887].

[68] B. Allanach, *SOFTSUSY: a program for calculating supersymmetric spectra*, *Comput.Phys.Commun.* **143** (2002) 305–331, [hep-ph/0104145].

[69] G. Belanger, F. Boudjema, A. Pukhov, and A. Semenov, *MicrOMEGAs 2.0: A Program to calculate the relic density of dark matter in a generic model*, *Comput.Phys.Commun.* **176** (2007) 367–382, [hep-ph/0607059].

[70] J. Casas, A. Lleyda, and C. Munoz, *Strong constraints on the parameter space of the MSSM from charge and color breaking minima*, *Nucl.Phys.* **B471** (1996) 3–58, [hep-ph/9507294].

[71] A. Kusenko, P. Langacker, and G. Segre, *Phase transitions and vacuum tunneling into charge and color breaking minima in the MSSM*, *Phys.Rev.* **D54** (1996) 5824–5834, [hep-ph/9602414].

[72] K.-I. Hikasa and M. Kobayashi, *Light Scalar Top at e+ e- Colliders*, *Phys.Rev.* **D36** (1987) 724.

[73] A. Djouadi, M. Muhlleitner, and M. Spira, *Decays of supersymmetric particles: The Program SUSY-HIT (SUspect-SdecaY-Hdecay-InTerface)*, *Acta Phys.Polon.* **B38** (2007) 635–644, [hep-ph/0609292].

[74] S. Bornhauser, M. Drees, S. Grab, and J. Kim, *Light Stop Searches at the LHC in Events with two b-Jets and Missing Energy*, *Phys.Rev.* **D83** (2011) 035008, [arXiv:1011.5508].

[75] M. Carena, A. Freitas, and C. Wagner, *Light Stop Searches at the LHC in Events with One Hard Photon or Jet and Missing Energy*, *JHEP* **0810** (2008) 109, [arXiv:0808.2298].

[76] M. Drees, M. Hanussek, and J. S. Kim, *Light Stop Searches at the LHC with Monojet Events*, *Phys.Rev.* **D86** (2012) 035024, [arXiv:1201.5714].

[77] S. Kraml and A. Raklev, *Same-sign top quarks as signature of light stops at the LHC*, *Phys.Rev.* **D73** (2006) 075002, [hep-ph/0512284].

[78] ATLAS Collaboration, G. Aad *et. al.*, *Search for pair-produced third-generation squarks decaying via charm quarks or in compressed supersymmetric scenarios in pp collisions at $\sqrt{s}$=8 TeV with the ATLAS detector*, arXiv:1407.0608.

[79] U. Baur and L. Orr, *Searching for $t\bar{t}$ Resonances at the Large Hadron Collider*, *Phys.Rev.* **D77** (2008) 114001, [arXiv:0803.1160].

[80] D. E. Kaplan, K. Rehermann, M. D. Schwartz, and B. Tweedie, *Top Tagging: A Method for Identifying Boosted Hadronically Decaying Top Quarks*, *Phys.Rev.Lett.* **101** (2008) 142001, [arXiv:0806.0848].

[81] W. Beenakker, R. Hopker, and M. Spira, *PROSPINO: A Program for the production of supersymmetric particles in next-to-leading order QCD*, hep-ph/9611232.

[82] M. Cacciari, G. P. Salam, and G. Soyez, *FastJet User Manual*, *Eur.Phys.J.* **C72** (2012) 1896, [arXiv:1111.6097].

[83] M. L. Mangano, M. Moretti, F. Piccinini, R. Pittau, and A. D. Polosa, *ALPGEN, a generator for hard multiparton processes in hadronic collisions*, *JHEP* **0307** (2003) 001, [hep-ph/0206293].

[84] A. Djouadi, J.-L. Kneur, and G. Moultaka, *SuSpect: A Fortran code for the supersymmetric and Higgs particle spectrum in the MSSM*, *Comput.Phys.Commun.* **176** (2007) 426–455, [hep-ph/0211331].

[85] D. G. Cerdeno and O. Seto, *Right-handed sneutrino dark matter in the NMSSM*, *JCAP* **0908** (2009) 032, [arXiv:0903.4677].

[86] D. G. Cerdeno, J.-H. Huh, M. Peiro, and O. Seto, *Very light right-handed sneutrino dark matter in the NMSSM*, *JCAP* **1111** (2011) 027, [arXiv:1108.0978].

[87] J.-J. Cao, K.-i. Hikasa, W. Wang, and J. M. Yang, *Light dark matter in NMSSM and implication on Higgs phenomenology*, *Phys.Lett.* **B703** (2011) 292–297, [arXiv:1104.1754].

[88] D. A. Vasquez, G. Belanger, C. Boehm, J. Da Silva, P. Richardson, *et. al.*, *The 125 GeV Higgs in the NMSSM in light of LHC results and astrophysics constraints*, *Phys.Rev.* **D86** (2012) 035023, [arXiv:1203.3446].

[89] A. Semenov, *LanHEP - a package for automatic generation of Feynman rules from the Lagrangian. Updated version 3.1*, arXiv:1005.1909.

[90] U. Ellwanger and C. Hugonie, *NMHDECAY 2.0: An Updated program for sparticle masses, Higgs masses, couplings and decay widths in the NMSSM*, *Comput.Phys.Commun.* **175** (2006) 290–303, [hep-ph/0508022].

[91] Particle Data Group, K. Nakamura *et. al.*, *Review of particle physics*, *J.Phys.* **G37** (2010) 075021.

[92] A. Davies, C. Froggatt, and A. Usai, *Light Higgs boson in the spontaneously CP violating NMSSM*, *Phys.Lett.* **B517** (2001) 375–382, [hep-ph/0105266].